THERMODYNAMICALLY CONSISTENT ANALYSIS FOR LITHIUM-ION BATTERIES

A Thesis

by

MURALI SRIVATSA CHAKRAVARTHY

Submitted to the Office of Graduate and Professional Studies of
Texas A&M University
in partial fulfillment of the requirements for the degree of

MASTER OF SCIENCE

Chair of Committee,	Partha P. Mukherjee
Committee Members,	Ying Li
	Sarbajit Banerjee
Head of Department,	Andreas A. Polycarpou

August 2017

Major Subject: Mechanical Engineering

ABSTRACT

An approach for the numerical modelling of Lithium Plating on intercalation electrodes with or without phase transition using a thermodynamically consistent (TC) solid-state transport is presented for a positive electrode (Nickel-Cobalt-Aluminum oxide) and a negative electrode (Lithiated graphite). The proposed method considers the positive electrode to be a single-phase regime and the graphite to consist of three phases, each with a Nernstian Equilibrium potential. The phase transition and volume fraction of the species are directly related through modifications to the Avrami's equation. A thermodynamically consistent approach is used to match experimental results to models at high C-rates (greater than 0.25C). The effect of using thermodynamically consistent approach on discharge/charge is obtained for varying performance characteristics (C-rate, size of particle). The visualization of phase change in graphite is captured through the assumption that each phase of graphite (LiC_6, LiC_{12} and LiC_{32}) are each represented by a sphere whose diffusivity is equal to the diffusivity of the phase. Lithium plating is considered to occur at negative overpotentials that are created locally, through low temperature or high C-rates and is formulated as being a Butler-Volmer type current density which is then directly correlated to the thickness of the Lithium plated metal layer. The effect of temperature and C-rate is observed in this study. C-rate and temperature have equal impact on the performance of the electrode and the formation of lithium plating on the surface of the electrode.

DEDICATION

I would like to dedicate this work to my family who have supported me all my life. I would not be in this position without the strength my family provides.

I would also like to thank my friends who have stuck by me through this tumultuous two years. A special mention to a few of them who have been a real inspiration with their dedication and spirit.

ACKNOWLEDGEMENTS

I would like to thank my committee chair, Dr. Partha P. Mukherjee, and my committee members, Dr. Ying Li and Dr. Sarbajit Banerjee for their guidance and support throughout the course of this research.

I would also like to mention my colleagues at the Energy and Transport Science Lab for always lending a helpful hand and to my friends at Texas A&M University and from back home. Lastly, thanks to my mother, father, sister and Sandy for their undying support and love.

CONTRIBUTORS AND FUNDING SOURCES

This work was supervised by a thesis committee consisting of Professor Partha P. Mukherjee and Professor Ying Li of the Department of Mechanical Engineering and Professor Sarbajit Banerjee of the Department of Chemistry.

All work for the thesis was completed by the student, under the advisement of Partha P. Mukherjee of the Department of Mechanical Engineering.

This research was supported in part by the faculty research initiation grant from Texas A&M University.

TABLE OF CONTENTS

Page

Page

LIST OF FIGURES

Page

Page

Page

LIST OF TABLES

Page

CHAPTER I

INTRODUCTION TO LITHIUM ION BATTERIES

Introduction

The world population is on the verge of facing one of the biggest energy crisis in the next decade. There is a large imbalance between demand and supply of energy already and this gap is only widening with growth of population, high energy consuming devices and an over-reliance on Electronics. To feed this demand, fossil fuels are currently being excessively used either through direct combustion or through the production of electricity. The inefficiency in the production of electricity through combustion is large.

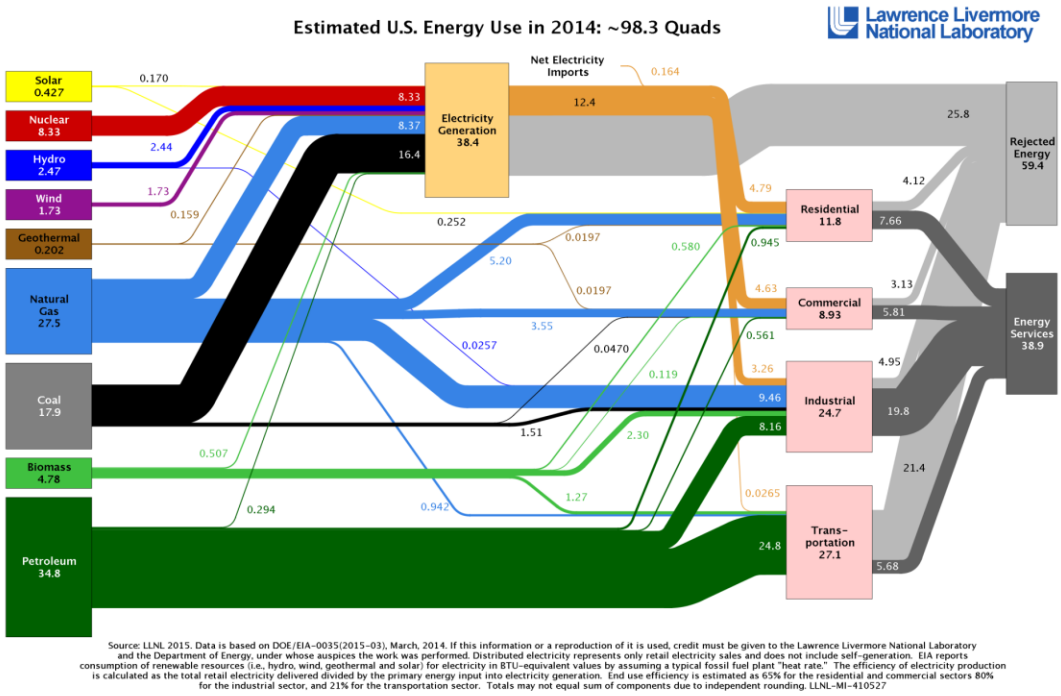

Figure 1: Energy consumption in the United States, reprinted from Lawrence Livermore National Lab[1]

Figure 1 above quite succinctly depicts the reliance the United States has on Petroleum and other fossil fuels.

One way to combat both the use of fossil fuels and the efficiency is using energy from renewable sources with solar, wind and geothermal energy being the most popular and efficient. The biggest hurdle in the use of renewable sources of energy was in the devices capable of storing such vast amount of energy at a reasonable cost. Secondly, there are major fluctuations in the source of renewable energy especially with solar and wind energy. A battery is one of the most commonly used devices for energy storage which solves both these issues. It is thus extremely important that a battery exists that is capable of storing large amount of energy. Its great specific energy and its recyclability[2] has led to it becoming a research focus as seen in Figure 2. The predominant use of batteries is in storage and release of energy and the battery does so through movement of electrons and ions. This is a simultaneous process unlike most other energy producing methods which have multiple intermediate steps that lead to generation of entropy and losses.

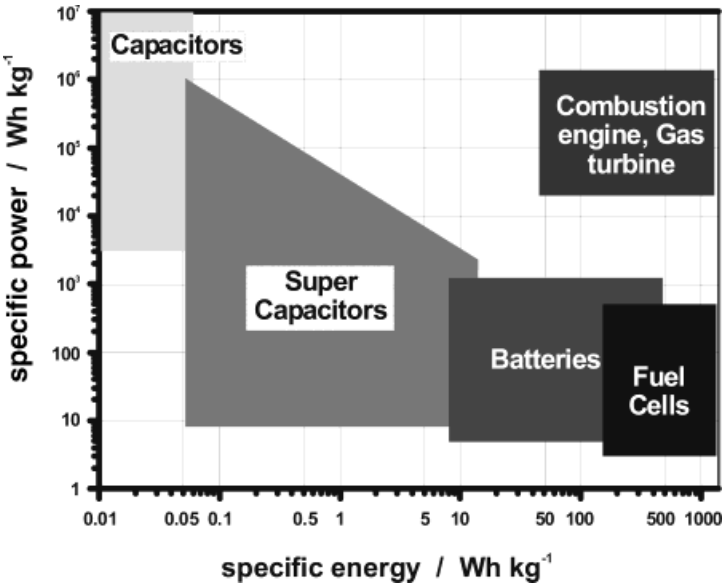

Figure 2: Ragone plot of various energy storage devices, reprinted from Winter and Brodd 2004[2]

Working principle of an electrochemical system

A battery, or an electrochemical cell usually consists of a positive electrode and a negative electrode immersed in an electrolytic solution (newer batteries are being made of solid-state electrolytes[3]) with a separator placed between them to only allow charged species to diffuse to the other electrode[4] but does not allow for the movement of electrons. The battery provides electric current through a reduction-oxidation reaction between the electrodes. One electrode gets reduced and the other, oxidized. This involves movement of charged species across the separator but also involves movement of electrons through an external connection between the electrodes. Electrons are only allowed to move through an external connection between the two electrodes leading to a current whose direction is opposite to the direction of the movement of the electrons. During

discharge, the anode undergoes an oxidation reaction and the cathode, a reduction reaction.

Typical Reactions at the electrode during discharge:

Cathode: $X + e^- \rightarrow X^-$ [Reduction reaction occurs as the cathode accepts the electron]

Anode: $X^- \rightarrow X + e^-$ [Oxidation reaction occurs as the anode releases an electron]

The positive electrode accepts electrons and the negative electron release the electron. At the same time, ions migrate from the anode to the cathode and either intercalate[5] through various means or precipitate[6], depending on the type of electrochemical cell involved. As mentioned earlier, rechargeable batteries involve the reversal of the cathode and anode reactions by the application of current externally in a direction opposite to discharge current direction. This is shown quite clearly in Figure 3 for a simple electrochemical system.

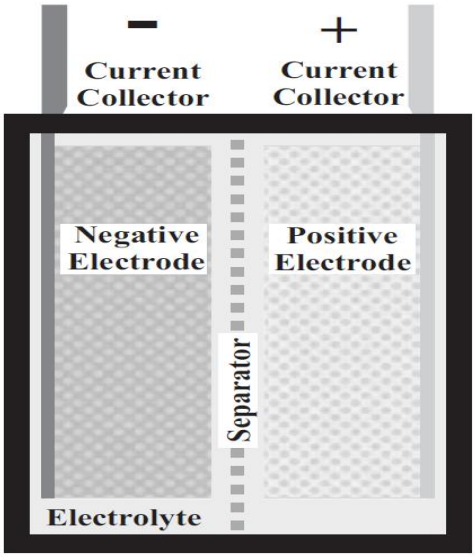

Figure 3: Schematic of an Zn-Cu electrochemical cell, reprinted from Rahn and Wang 2013[7]

Classifications of batteries

The battery, thus is a self-contained chemical storage device which can, on demand be converted to electric energy by the application of electric current. They are divided into three main categories[7]. Primary batteries are battery systems in which the electrochemical reactions which occur are all mostly irreversible. This means that the battery is sold in a charged condition can only be discharged once and then are discarded (Alkaline, Zinc-air). Secondary batteries are those that involve reversible electrochemical reactions i.e. the reactions that happen during discharge can be reversed by inverting the direction of the applied current. Although these reactions are not completely reversible and do wear out after cycling multiple times[8-11], they are a better option in applications that require use of batteries on a regular basis. Examples of secondary battery systems include Lead Acid, Lithium Ion and Nickel-Cadmium. Lastly, Speciality batteries are primary batteries that are produced in limited quantities and are made specifically for a certain purpose.

Background of battery development

The Renewable energy is mostly in need of rechargeable or secondary batteries came into prominence in the 19^{th} century[12]. Until the 1950s, primary batteries such as Zinc-Carbon was used mostly for its safety and portability. Lead Acid batteries were the first to be implemented in a large scale followed by other chemistries.

Nickel-Cadmium system was the next to come into commercial prominence but was not environmentally friendly and was thus replaced by Nickel-Metal-hydride system which

was very similar chemically but was environmentally friendly. At the same time, significant research was being done in the Lithium ion battery research. Lithium is the lightest electropositive metal and leads to high specific energy. There were multiple problems related to Lithium ion battery systems. Primary among them was the inherent instabilities due to high reactivity of Lithium and dendrite formation leading to short circuiting[13]. A lot of these problems have been solved by using Lithium oxides instead of the Lithium metal as electrode. Another issue with Lithium ion batteries is the significant volume changes[14] during operation due to intercalation and de-intercalation of Lithium ions in the electrodes giving rise to stresses and capacity fade[15]. These issues have been resolved to an extent using carbonaceous material intercalation. However, despite these problems, Lithium-ion has started to really dominate the market currently due to its low weight and high theoretical capacity. They also can retain the charge over long durations. The biggest issue is still the safety of batteries. Temperature strongly dictates Lithium ion battery performance and thermal runaway is a leading cause of catastrophic failure. Other safety issues include short circuiting due to dendrite formation and over-charging leading to Lithium plating.

Lithium ion batteries

Lithium ion batteries work through intercalation and de-intercalation of Lithium ions[16]. The most commonly used negative electrode is Carbon or Li_xC_6 but the positive electrodes usually vary. There have been many positive electrodes but the ones with the

most focus are $LiFePO_4$ and NMC (Nickel-Molybdenum-Cobalt Oxide) electrodes[17-20].

The active material(AM) is bonded to current collectors (copper for anode and aluminum for cathode) and are separated by a polymer based separator that isolates the two electrodes electrically but allows for ion species migration.

Intercalation is the process through which Lithium ions get inserted into the electrode during the discharge/charge process. During discharge, the negative electrode is oxidized and Lithium de-intercalates from the anode structure while releasing electrons. The cathode accepts the Lithium ion and the cathode intercalates and to ensure charge neutrality, it also needs to accept an electron. During charge, the process is reversed. The cycling process of intercalation and de-intercalation leads to stresses created due to change in the volume of the electrode, lowering the life of these battery systems.

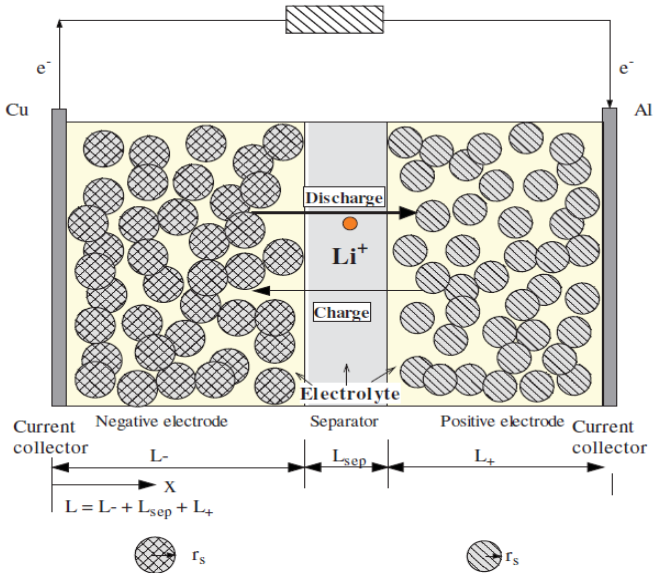

Figure 4: Schematic of 1D Li-ion cell, reprinted from Fang, Kwon et al. 2010[21]

Figure 4 shows a schematic of a 1D Lithium ion cell including the direction of the ions during charge and discharge. The cell is 3 dimensional but only 1D movement of electrolyte and ions is considered for computational simplicity.

Majority of the Lithium ion research goes into understanding the intercalation process that occurs in these electrodes[22-24]. The electrochemistry that is associated with intercalation can help in designing a better battery system. The models that are most prevalently used does have to have experimental data that is used to fit the experimental data to model data. This helps in obtaining electrode parameters which can then be used to understand the behavior of the battery. A lot of assumptions are made with respect to the material properties of the electrode and electrolyte based on prior data and theoretical formulation that can accurately predict the behavior but does not necessarily make sense physically.

CHAPTER II

LITERATURE REVIEW

Lithium ion batteries have come a long way from being extremely unsafe to becoming one of the most commonly used battery configurations, especially in smaller appliances such as cell phones, laptops etc. The greatest advantage of these batteries is the fact that they have a high-energy density, low self-discharge and low weight/energy delivered. This has led to a large amount of research going into battery chemistry i.e. trying to find optimum electrode materials that provide even higher energy density and energy storage capabilities and better cycling capability. They are even being considered for larger energy storage applications such as Hybrid Electric Vehicles(HEV) and Plug-in Hybrid Electric Vehicle(PHEV). This would mean replacing the Lead-acid batteries that are ubiquitous in the automotive and power grid applications. Apart from experimental research, computational research on understanding the physics of electrochemistry and the insertion of Lithium ions in the electrodes are of prime importance since accurate computational models can be used with far more robustness than experimental models. The ability to tweak parameters and understand the effect they may be having on the electrochemistry without creating new battery configurations thus becomes the most viable option available.

One of the hottest research topics has been to understand the solid-state transport of the Lithium across the electrode, either positive or negative. There are numerous papers that try to model the electrochemical system making assumptions[25-30] (electrode as

sphere, electrolyte properties not varying, concentration gradient based solution vs chemical potential as a driving force, single particle model vs pseudo 2-D model).

The earliest attempt to model an electrochemical system was done by Doyle et al.[27]. They tried to create a model that would match the Galvanostatic charge and discharge curves. They assumed the electrode to consist of spherical particles of a given radius (assumed at that point but later verified through a scanning electron microscope) and diffusion was the main source of movement of ions. This work was seminal in the Lithium ion modelling community as most work that came after adopted their methodology for ion transport and charge transport.

Santhanagopalan et al.[10] were the first to assume a single particle model. In this approach, the whole electrode is simplified to be a single sphere of electrode material and the porosity of the single particle is representative of the porosity within the electrode. Additionally, the surface area used in the finding the electrochemical current density uses a specific area (surface area of particle/Volume of the electrode) to represent the complete surface area of the electrode. The use of the specific area helped with the computational difficulties of using two length scales i.e. the particle length scale which is in the order of μm and the electrode length which is in the order of mm.

Several other works[8, 11, 31-33] then used the concept of single particle model and expanded it to understand capacity fade, thermal effects, effect of stress and the accuracy of single particle with other models. The consensus was that although the single particle model was computationally simple, it did not reflect accurately the physics inside

the electrode. Additionally, a single particle model does not consider the effects of electrolytes and its breakdown at high temperature and high C-rate applications.

With the advent of technology, more physically accurate models were developed. These models were computationally extremely demanding but were providing satisfactory match with experimental results at low temperature and high C-rates which are thermodynamically were the most non-ideal and required the use of non-equilibrium thermodynamics and the understanding of nanoscale mechanics that occur within an electrode and how it might change with change in environmental and physical parameters.

One of the biggest assumptions that is made when it comes to solid-state transport of Lithium ions is that the diffusivity of the Lithium intercalating is the same[34-37]. If you consider the electrode to be an isotropic sphere, then during discharge, Lithium is extracted from the anode and inserted into the cathode. The Lithium is assumed to create a flux on the surface of the sphere and then diffuse into the electrode for the cathode and there is a negative flux created in the anode and Lithium ions are dragged out of the electrode from the inside. This is mostly done for computational ease but it has been observed in literature that the diffusivity is never a constant value[30, 38, 39]. The Srinivasan and Newman model[30], especially has been used as a staple for modelling electrochemical behavior for the greater part of 10 years since it was published in 2004 but there -have been multiple arguments/inconsistencies with the model. The equilibrium configuration of Li intercalated in the electrode materials are usually defined by open circuit potential profile[40] as a function of intercalated Li. By default, open circuit

potential is related to Nernst equation which says that the Open Circuit potential(OCP) E is defined as

$$E = E^0 + \frac{RT}{F}\ln(\frac{Cs\max - Cs}{Cs}) \quad (1)$$

where E^0 is a reference state, usually a dilute solution. The Srinivasan, Newman model instead depend on a fit of the experimental Open Circuit Potential which may not necessarily be Nernstian in nature. Especially when it comes to electrodes that experience a phase change which are plateaus in Voltage in the OCP vs State of Charge(SoC) profile. $LiFePO_4$ and LiC_6 are phase changing materials and although there are models that try to fit a curve to represent the OCP[39], they are not founded on physics. Most models assume only 2 phases to exist, the intercalated Lithium and empty spaces which intercalating Lithium ions can fill. This is not entirely true as diffraction patterns have shown the presence of various stages of intercalated Lithium[41]. In Carbon, which is of prime focus, there can be multiple arrangements of intercalated lithium depending on the extent of intercalation. The different phases can be accounted for in two different ways:

1. Find the potential that drives the intercalation process as a function of the OCP and attribute each phase with a volume fraction. Assumptions about the conductivity of each phase, initial diffusion coefficients are made.

2. In this method, the phase change boundary[42] is tracked and would involve solving a moving boundary problem, which would be computationally intensive and would not really be helpful for single phase regions[43].

The next question is how many phases exist and which phases are important for consideration? Additionally, how is ionic and electronic transport in them occurring? From Gibbs Phase rule, the degrees of freedom is evaluated as F = C-P-2[44, 45], where C is the number of components and P is the number of phases. A two-phase region would involve no degrees of freedom and thus voltage would remain constant. These regions can be isolated in the OCP of an electrode or at low C-rates. The plateau region can only be observed at low C rates as the time constants for these phase transformation is generally very slow[46]. From the spectroscopy results, 2 phases i.e. LiC_6 and LiC_{12} are clearly evident[41] but beyond that, they are only able to speculate as the intensity isn't strong enough to capture phase change. This occurs due to lack of resolution in the device itself or the small quantities of the other phases.

At least 4 phases have been suggested but experimental evidence have not definitely proved these suppositions.

There are a multitude of factors that are changing with changing SoCs. Component diffusion, conductivity of the electrode, OCP of single phase regions would change depending on what phase is present, the chemical kinetics would also be affected by the intercalation. Most assume it to be constant over the discharge cycle, some assume that it change with intercalation as expressed by the thermodynamic factor[38], the Bruggeman-type relations[47] or just fit it according to experimental data.

Ozukhu et al.[48] have observed the method of discharge of LiC_6. When the Li is extracted out, LiC_{12} nucleates from the pure LiC_6. And be in phase equilibrium with LiC_6 at one of the voltage plateaus, until the point where all LiC_6 is consumed and are

transformed to the LiC_{12} phase. While Ozukhu goes on to describe the other phases such as LiC_{18} and $LiC_{27,}$ only 3 phases have been experimentally found, 2 of which conclusively and another from plausible extrapolation of results. So, it would be ideal to only consider 3 phases, as has been done in other works[46].

Current induced Transition from particle-by-particle[49-51] to concurrent intercalation in phase separating battery electrodes by Li et al.[52] goes mostly into understanding what leads to the transition from a particle-by-particle intercalation to bulk transfer. The active population, which is the number of molecules that are actively participating in the intercalation process, is important because it can dictate multiple electrode properties and can affect capacity fading. If intercalation is only concentrated in a small region, it would lead to a hotspot in terms of local current density and will lead to fracture and increase the rate of capacity fading. The study in this paper is with respect to Lithium Iron Phosphate (LFP) electrodes alone which has 1 phase separating region as evidenced by the near constant OCP curve. The assumptions in earlier works regarding the uniformity in size of all the active particles leads to a current density which may not be accurate. The experimental results showed that the concurrent behavior is usually observed at high C-rates but the author does not believe that cycling behavior and C-rate are the only effects resulting in this transition. Interestingly, the author removed the electrolyte before stabilization so that there is no inter-particle lithium transport occurring. They noticed in their experiment that irrespective of the electrode charging current, a small minority of the active particles carry most of the current during charge and in contrast, on discharge, the number of active particle had a heavy dependence on rate of discharge. It

is hard to prove this conclusion through voltage curves as the same cell voltage can be obtained from multiple cathode and anode overpotentials. In discharge, a definite transition can be seen between the two effects but in charging, there is no observation of concurrent transfer of current. This would mean that the local current density in charge is higher than the current density on discharge. As for understanding the concepts of the transition, they assume LFP to have local transformation barriers, energy levels that need to be reached before the Lithium particle becomes active. Although the experiments would suggest that this barrier is unequal for charge and discharge, the author takes it to be constant and explains the heterogenous nature through the Butler-Volmer equation. The driving force for the movement is the difference in chemical potential, the derivate of free energy to the transformation barrier. The author defines a I_{crit} that defines the critical value of current at which point 65% of the particles have lithiated. Beyond this point, current density increases heavily with rate, something the thermodynamically consistent approach also agrees with although it does so through the solid-state diffusivity as compared to the current density. On further lithiation, the active population saturates and all the ion transfer would be concurrent. This is an alternate method to understanding the intercalation. The I_{crit} would not figure at low C-rates and is implicit in understanding whereas having a fit on the diffusivity might work for high C-rates but might not be correct, physically at lower C-rates. This also necessarily means that the overpotential doesn't increase beyond this point, it only increases the current density. Another factor for consideration is that intercalation might depend on the proximity to the carbon network as these particles are more likely to reach the transformation barrier and lithiate as compared to particles that

are fair ways away from the carbon network. In conclusion, a good way to improve concurrent transfer would be to either decrease the transformative barrier through additives or by reducing reaction rate constant and exchange current density.

Phase transformation dynamics in Porous battery electrodes by T.D Ferguson and M.Z.Bazant[53] is a companion paper to [54]. The author goes over understanding the phase transition for Iron phosphate (single plateau) and graphite (multiple plateaus). This paper goes understanding low C-rate behavior of LFP and graphite but this isn't of much use to us since factors such as electrolyte concentration, overpotential due to diffusion and phase change behavior being particle-by-particle but it helps understand the way one could model the OCP and the chemical potential profile according to the electrode properties. The first thing to note was that particles in the electrodes are assumed to be normally distributed and two parameters that are fit are the mean size of the particle and standard difference of particles that are offset from the mean.

The reference voltage(V_0) is defined in the middle of the plateau and is an average of the voltage of the plateau by consequence and the chemical potential ($V_{eq}=V_0 - \mu/e$) is defined and the overpotential is given by = $V-V_{eq}$ which then goes into a generalized Butler-Volmer equation to give the reaction rate. Multiple parameters such as electrolyte diffusivity, active material loading, porosity, thickness, tortuosity) are all estimated which might not be accurate as these factors affect the performance curve at high C-rates. The earliest way to recognize phase change was to assume the shrinking core model[30, 55], which is hard to prove physically and needs multiple parameters to be fit every time a solution needs to be obtained.

For graphite, a homogenous energy model is created with some minima corresponding to each phase change and the height of the barrier corresponding to how easy it is for the particle to lithiate in this fashion. By setting the transformation barrier[54, 56], 2 phase behavior can be modelled effectively, each phase having its own free energy, chemical potential and overpotential and the relative energy giving a sense of how many of the active particles are in which phase. The sum of the local current densities of each particle will help in finding the overall current density of the system. There is however an interaction energy between the two phases, which recognizes the interaction that two adjacent particles will have with each other and how that will affect the lithiation behavior. This interaction energy also applies to particle vacancy dipoles which can account of partially filling layers and the affinity for the electrode to choose one phase over another due to limited availability. This is an extremely useful piece of information which can be used in my research to correctly model phase change behavior and for it to be independent of fitted parameters such as the OCP curve, the OCP curve will be a consequence of these factors.

There have been multiple papers that have touched upon thermodynamically consistent approaches[38, 57-59] to finding a model that closely matches experimental results. The thermodynamically consistent approach tries to relate the diffusivity with the amount of active population. It is a reasonable assumption that diffusivity of the solid-state does not remain constant as the cell charges/discharges. It changes with various factors such as temperature, state of charge, elastic strain on the electrode and on particle size. The thermodynamically consistent approach tries to bridge the gap between

modelling and physical processes by taking these changes into account. The primary paper under consideration has been the thermodynamically consistent analysis of Nickel-Cobalt-Aluminum oxide(NCA). The paper considers a thermodynamic constant which is related to the change of the activity of a species against the change in the state of charge. An additional term to relate the bulk movement of Lithium ions at a highly lithiated state further adds to the accuracy of the model in stochastic sense.

As for Lithium plating, there has been significant research done with Lithium Plating[60-64], especially on negative electrodes. Lithium Plating usually occurs due to deposition of Lithium on the surface of the electrode in a permanent reaction. The identification of plating and the amount of plating that occurs has been very difficult. Various in-situ means have been used to find the amount of plating, either at room temperature and overcharge or at low temperatures[63, 65-69]. Lithium plating is detrimental for two reasons, it reduces the total amount of Lithium available to be intercalated, thereby reducing the capacity and secondly reduces the interfacial area available for Lithium ions that is migrating through the electrolyte to de-intercalate, thereby reducing performance.

The modelling of Lithium Plating in electrodes is quite well established. A Butler-Volmer negative overpotential is used[70] to describe plating and as the thickness of the lithium plated material increase, so does the overpotential associated with Lithium Plating. This thus eats away the total current that is being supplied to the cell.

Lithium plating can occur at low temperature situations where the diffusivity is low and that causes a build-up of Lithium ions at the surface of the electrode but with no

room for movement and the only option in this situation is the lithium being plated on the surface of the electrode. Lithium plating can also happen at high C-rate application where the driving force is so large and the diffusion low that it leads to plating. Lastly, Lithium plating can occur due to a localized increase in current density which provides so much energy at a localized point to a Lithium ion without the option of migration and that leads to Lithium getting plated on the surface.

There has been some debate over the mechanism or initiation of plating. There could be an accumulation of Lithium ions at the interface. This coupled with slow diffusion in the solid-state then leads to a large overpotential on the electrode and causes Lithium plating to occur[71]. The other concept is of a plating potential criteria[72-75]. This says that the plating is controlled by its overpotential which is then attributed to a Butler-Volmer type current density relating to plating. This criterion says that if the plating overpotential drops below the Li^+/Li voltage which is considered to be 0 V, it leads to plating or lithium deposition on the surface of the electrode.

CHAPTER III

METHOD DESCRIPTION

Introduction

The model was created in C++ using the formulation provided by Newman et al.[27] to begin with and then expand the formulation to consider thermodynamically consistent diffusion as provided by Bernardi et al.[38] that has been provided for NCA but also expands the derivation for thermodynamically consistent model for 1 phase into 3 phases (applied to graphite phases). Lastly, the Lithium plating was added by using the framework provided by Ge et al.[70]. The basic equations are provided below. The model is a half-cell consisting of Nickel-Cobalt-Aluminum oxide and Carbon as cathode respectively and Lithium plate as anode. Since the Lithium metal plate electrode is a reference electrode in Lithium ion battery chemistries, the behavior observed in the model can be wholly attributed to the electrode under consideration. Half cells are primarily used when new electrodes are being tested or when the behavior of only one electrode is being tested.

There are two sections to this Chapter. The first goes over the general formulation associated with the code developed. Also mentioned is the boundary conditions at the anode-separator boundary and the cathode-current collector interface. The second section goes over the parameters assumed or given in literature.

Model description

The four main equations (Eq. 2-5) are coupled non-linear differential equations[10, 76] that are solved to determine the 4 dependent variables ϕ_s, ϕ_e, c_s and c_e which correspond to the chemical potential in solid phase, chemical potential in electrolyte phase concentration of solid phase and the concentration of electrolyte phase. All other variables are obtained from these 4 parameters and/or assumed/given in literature.

Conservation equations

1. Conservation of Species – Fick's Law

   A radial isotropic sphere is considered to represent the electrode and the surface area of the electrode is the same as the surface area provided by the physical electrode. The porosity is quite an important feature because that effectively increases the surface area available for intercalation.

$$\frac{\partial c_s}{\partial t} = \frac{1}{r^2}\frac{\partial}{\partial r}\left(D(r) r^2 \frac{\partial c_s}{\partial r} \right) \tag{2}$$

   where the D(r) is the solid-state diffusivity that is corrected to obtain a result that more closely matches experimental results.

2. Conservation of Species – Electrolyte

   The Li^+ ions are conserved in the electrolyte as well and is given by the form

$$\varepsilon \frac{\partial c_e}{\partial t} = \frac{\partial}{\partial x}\left(D_e \frac{\partial c_e}{\partial x} \right) + \left(\frac{1 - t^+}{F} \right) j \tag{3}$$

which shows that in an electrolyte, the conservation of species is through diffusion of species and through an electrochemical reaction due to a volumetric current source term j.

3. Transport of Electrons in Solid Phase

   This equation is related to Ohm's law and charge conservation in the solid phase.

$$\sigma_{eff} \frac{\partial^2 \phi_c}{\partial x^2} = j \tag{4}$$

4. Charge Conservation in electrolyte phase

   This equation is related to Ohm's law and conservation of charge in the electrolyte phase. Unlike the Solid phase which only has a component, there is a migration term and a diffusion term due to concentration gradient in the charged species present in the electrolyte. There is no temporal term in this equation because charge neutrality is assumed.

$$\frac{\partial}{\partial x}\left(\kappa_{eff} \frac{\partial \phi_e}{\partial x} + \kappa_D^{eff} \frac{\partial (\ln C_e)}{\partial x} \right) + j = 0 \tag{5}$$

Butler-Volmer electrochemical reaction

Here, the volumetric current source term j is representing the electrochemical reaction per unit volume of the electrode. Unlike other chemical reactions, electrochemical reactions occur at the electrode/electrolyte interface and hence the volumetric source term is

related to the surface reaction current density through the Butler-Volmer Reaction and is given by

$$j = ai = a\left(k_c c_s^{1/2} (c_s^{\max} - c_s)^{1/2} c_e^{1/2} \left[e^{\frac{F}{2RT}(\phi_c - \phi_e - E)} - e^{\frac{-F}{2RT}(\phi_c - \phi_e - E)} \right] \right) \quad (6)$$

where c_s is solved in equation (2) and ϕ_c and ϕ_e are solved with equations (4) and (5) simultaneously with the Butler Volmer equation.

Boundary conditions

Appropriate Boundary conditions are necessary to solve these equations. The boundary conditions for the equations are provided below.

1. Species Conservation in Electrode:

   At particle center r=0: $-D_{c,0}\nabla c_s = 0$ (7)

   At particle surface r=R: $-D_{c,0}\nabla c_s = \frac{jR}{3\varepsilon_c}$ (8)

2. Species Conservation in Electrolyte:

   Reference electrode-Separator: $-D_e \nabla c_e = \frac{(1-t^+)}{F} J$ (9)

   Electrode – Current collector: $-D_e \nabla c_e = 0$ (10)

3. Charge Conservation in Solid-state

   Reference Electrode Separator: $-\sigma^{eff} \nabla \phi_s = 0$ (11)

Electrode – Current Collector: $-\sigma^{eff}\nabla\phi_s = J$ (12)

4. Charge Conservation in Electrolyte phase

Reference Electrode – Separator: $\phi_e = 0$ (13)

Electrode – Current Collector: $-\kappa^{eff}\nabla\phi_e = 0$ (14)

Since the reference electrode of Lithium metal plate has such a high conductivity, it is usually inconsequential in the results obtained apart from a small jump in the overpotential which is adjusted in the code.

Thermodynamically consistent approach

For the Thermodynamically consistent model, the thermodynamic factor[38] is derived which corrects the solid-state diffusivity for bulk movement and the change it has with SoC. Thermodynamic factor is given by $\left[1+\frac{\partial \ln \gamma_I}{\partial \ln x_I}\right]$ and the new Fick's law with thermodynamic factor considered looks like the following

$$\frac{\partial c_s}{\partial t} = \frac{1}{r^2}\frac{\partial}{\partial r}\left(\frac{D_{IS}}{1-x_I}\left[1+\frac{\partial \ln \gamma_I}{\partial \ln x_I}\right]r^2\frac{\partial c_s}{\partial r}\right) \quad (15)$$

and the thermodynamic factor is found by fitting the OCP of the phase under consideration as a modification of the Nernst equation[38].

The formulation of the data is quite well explained by Bernardi et al.[38]. For the sake of brevity, the following result was directly obtained from the paper.

$$\left[1+\frac{\partial \ln \gamma_I}{\partial \ln x_I}\right]=1+\frac{1}{RT}\sum_{k=2}^{9}\Omega_k(k-1)k\left[x_S^{k-1}-x_S^{k}\right] \tag{16}$$

where x_I is the SoC of the phase being considered and x_S is the number of sites available for intercalation divided by the theoretical total number of sites. If only 2 species are intercalating, the fraction of empty sites is given by $x_S=1-x_I$

The fitting parameters Ω_k can be obtained by fitting the OCP of the phase across the SoC that it is active in as an extension of the Nernst equation such that

$$E_{ref}=E_{ref}^{0}+\frac{RT}{F}\ln\left(\frac{1-x_I}{x_I}\right)+\sum_{k=2}^{9}\Omega_k k(1-x_I)^{k-1} \tag{17}$$

The first half is the ideal chemical potential and the second half, which includes the series expansion[77], is the excess chemical potential that is related to excess chemical potential. If the OCP curve can be fit to a formulation similar to the equations provided above, the thermodynamically consistent solid-state diffusivity can be obtained.

Lithium plating

For Lithium plating, a Butler Volmer equation very similar to the one that describes the surface electrochemical reaction current source term is considered. The total electrochemical reaction current density is being split into the intercalation source term and the other goes into plating of Lithium on the surface of the electrode[70]. Plating

reaction only occurs when the overpotential becomes negative leading to a reversal of charge. Therefore, to summarize, $j = j_1 + j_2$

$$j_1 = j_{0,1}\left(\left[e^{\frac{F}{2RT}(\phi_c - \phi_e - E_1 - \Delta\phi_{film,1})} - e^{\frac{-F}{2RT}(\phi_c - \phi_e - E_1 - \Delta\phi_{film,1})} \right]\right) \quad (18)$$

for the primary intercalation reaction, where $j_{0,1}$ represents the exchange current density for the electrochemical reaction.

$$j_2 = \min\left\{0, j_{0,2}\left(\left[e^{\frac{F}{2RT}(\phi_c - \phi_e - E_2 - \Delta\phi_{film,2})} - e^{\frac{-F}{2RT}(\phi_c - \phi_e - E_2 - \Delta\phi_{film,2})} \right]\right)\right\} \quad (19)$$

For the lithium plating reaction and note, again that a min function has been added to make sure that plating only occurs when the overpotential is negative. Relations for $j_{0,1}$ and $j_{0.2}$ are provided by Ge et al.[70] and no modifications were made to them.

Although ϕ_c and ϕ_e are solved normally and don't change for the two reactions, the 2 biggest differences between the overpotential of the primary reaction and the secondary Lithium plating reaction is that OCP of the primary reaction is given by the Nernst equation whereas OCP of the lithium plating reaction is 0 i.e. E_1 = OCP of Electrode under consideration and E_2=0.

There is a change in the thickness of the lithium on the surface, $\Delta\phi_{film}$, that is a time evolving potential created by the growth of the plated lithium metal film and is given by

$$\frac{\partial \delta_{film}}{\partial t} = \frac{j_2 M}{\rho F} \tag{20}$$

$$\Delta \phi_{film,k} = j_k R_{film} \tag{21}$$

where $R_{film} = \frac{\delta_{film}}{\kappa_{film}}$, δ_{film} being the thickness of the film at any instant and κ_{film} is the conductivity of the film.

Arrhenius temperature dependence

The equations were solved for different temperatures and different C-rates. An assumption made in this study is that the temperature of the model cell whole charging or discharging does not change when kept in the environmental chamber[70, 78]. The factors that affect the cell performance are the effects of temperature on the conductivity of the solid-state, conductivity of the electrolytic phase, junction potential conductivity, rate constant of the electrochemical reaction and diffusion of the solid-state. All these factors are either incorporated in their fit functions or can be attributed through the Arrhenius temperature relation given by:

$$X_T = X \exp\left(\frac{E_{a,X}}{R} \left[\frac{1}{T_0} - \frac{1}{T} \right] \right) \tag{22}$$

where X is the parameter under consideration at reference temperature T_0. X_T is the parameter at temperature T and $E_{a,X}$ is the activation energy of the parameter that attributes the sensitivity of the parameter with change in temperature[79].

Electrolyte properties

The electrolyte properties that are obtained through fitting experimental data[80] can be seen published below.

The electrolyte diffusion coefficient of $LiPF_6$ is fit by the equation

$$\log_{10} D_e = -4.43 - \frac{54}{T-(229+5c_e)} - 0.22c_e \tag{23}$$

The liquid phase ionic conductivity which also has a dependence on temperature and electrolyte concentration is given by the form

$$\sqrt{\frac{\kappa(c_e.T)}{c_e}} = \kappa_{0,0} + \kappa_{0,1}T + \kappa_{0,2}T^2 + \kappa_{1,0}c_e + \kappa_{1,1}c_eT + \kappa_{1,2}c_eT^2 + \kappa_{2,0}c_e^2 + \kappa_{2,1}c_e^2T \tag{24}$$

where the parameters $\kappa_{i,j}$ is fit based on the values obtained in [80].

The liquid phase junction potential[81] which is given by

$$\kappa_{junc} = \frac{2RT\upsilon}{F} \tag{25}$$

where $\upsilon = 0.601 - 0.24c_e^{1/2} + 0.982\left[1-0.0052(T-294)\right]c_e^{3/2}$ (26)

The effective values of the diffusivity, conductivity and junction potential of the electrolyte are affected by intrinsic properties such as tortuosity.

$X_{eff} = X\frac{\varepsilon}{\tau}$ where ε is the porosity of the liquid phase and τ is the tortuosity. In some references, the same formulation can be seen as $X = X_{eff}\varepsilon^{brug}$ where brug is the Bruggeman constant.

Graphite phase change model

Phase change has been incorporated from Gallagher et al.[46, 82]. The equations related to phase change are covered in the section below.

Phase change has been spoken about in earlier sections. Graphite has multiple phases[5, 41, 43, 46, 47, 83]. In this study, 3 phases are assumed to exist, namely LiC_6, LiC_{12} and LiC_{32}. Each phase is attributed to one plateau in the Open circuit potential curve of graphite.

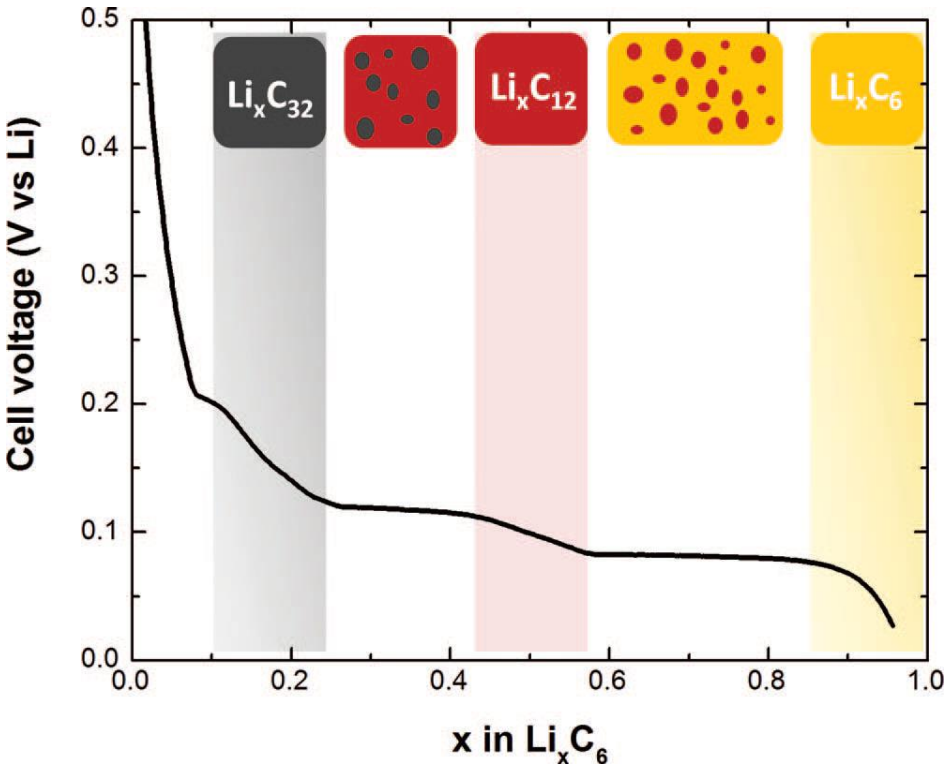

Figure 5: Open circuit potential of lithiated graphite, reprinted from Bernardi, Chandrasekaran et al. 2013[38]

In this study, 3 phases are considered as seen in Figure 5. The starting state involves LiC_6 exclusively present. As de-lithiation occurs, LiC_6 is transformed to LiC_{12} and then from LiC_{12} and LiC_{32}. Reaction rate for phase change between any 2 phases j and k is given by

$$R_{jk} = k_{s,jk}\varepsilon_{s,j}\Delta c^{*}_{s,j}H(\Delta c^{*}_{s,j}) \tag{27}$$

where $\Delta c^{*}_{s,j}$ is the supersaturated driving force that causes nucleation and phase transformation.

The rate of change for each phase is given by the following relations:

$$\frac{\partial \varepsilon_{s,1}}{\delta t} = R_{21} - R_{12} \tag{28}$$

$$\frac{\partial \varepsilon_{s,3}}{\delta t} = R_{23} - R_{32} \tag{29}$$

$$\varepsilon_{s,1} + \varepsilon_{s,2} + \varepsilon_{s,3} = 1 \tag{30}$$

Each phase has an electrochemical reaction current density which only operates in regions that occur after the first threshold supersaturation limit is reached.

$$i_{n,j} = i_{0,j}\left(\frac{c_e}{c_{e,ref}}\right)^{0.5}\left(\frac{c_{s,\max} - c_{s,j}}{c_{s,\max} - c^{0}_{s,j}}\right)^{0.5}\left(\frac{c_{s,j}}{c^{0}_{s,j}}\right)^{0.5}\left\{\exp\left[\frac{F}{2RT}\eta\right] - \exp\left[\frac{-F}{2RT}\eta\right]\right\} \tag{31}$$

$$\eta = \phi_s - \phi_e - U_s \tag{32}$$

where U_s remains the same for all three phases. Local equilibrium is assumed to exist between all the three phases. With the current density given, the flux related to each phase is calculated and thus the total de-lithiating flux.

Model parameters

These models based parameters are either assumed, derived from known values or fit to experimental results. The parameters are not constant for NCA and graphite as these properties are based on experimental results that were used by the initial author to fit parameters.

Tables 1,2 and 3 will include all the parameters that would be used to run the code for NCA and graphite. Phase specific information for graphite is in Table 4 and finally the parameters essential for plating such as activation energy and the reference values for temperature sensitive parameters can be found in Table 5.

Table 1: Common properties between all the half-cells considered

Properties	Unit	Value
Temperature	K	298
Initial $LiPF_6$ concentration	$molm^{-3}$	1150
Bruggeman co-efficient		1.5
Lithium metal exchange current density	A/m^2	8.5
Faraday's constant	C/mol	96487
Universal Gas constant	J/mol-K	8.314
Radial shells for solid-state particle		20
Total number of cells in separator		8
Total number of cells in electrode		20

Table 2: Electrochemical cell properties for NCA

Electrochemical cell properties	Unit	NCA positive half-cell
Volume Fraction of active material, ε		0.4676
Volume Fraction of liquid phase, ε_2		0.3382
Electronic conductivity of AM[84]	Sm^{-1}	0.05
Lithium diffusion coefficient in AM, D_s	m^2s^{-1}	5e-15
Charge-transfer rate coefficient k	$Am^{-2}(m^3mol^{-1})^{3/2}$	2.3e-3
Maximum concentration of active material	mol of Li/m^3	49195
Initial Concentration of AM, y^0		0.5173
1C cell current density	A/m^2	10.27
Particle size	μm	7.5
Separator thickness	m	10e-6
Separator volume fraction		0.46
Electrode thickness	m	25e-6
Transference number of Li^+ in liquid, t^+		0.363
Specific interfacial area	m^{-1}	196000

Table 3: Electrochemical cell properties for graphite

Electrochemical cell properties	Unit	Graphite negative half-cell
Volume Fraction of active material, ε		0.495
Volume Fraction of liquid phase, ε_2		0.384
Electronic conductivity of AM[46]	Sm^{-1}	5
Charge-transfer rate coefficient k	Am^{-2}	0.3
Maximum concentration of active material	mol of Li/m^3	31200
1C cell current density	A/m^2	22
Particle size	μm	10
Separator thickness	m	50e-6
Separator volume fraction		0.384
Electrode thickness	m	55e-6
Transference number of Li^+ in liquid, t^+		0.363
Specific interfacial area	m^{-1}	2401000

Table 4: Phase specific properties of graphite

Properties	Unit	Phase 1, LiC_6	Phase 2, LiC_{12}	Phase 3, LiC_{32}
Initial lithium fraction		0.99	0.01	0.01
Solid-state diffusivity	m^2s^{-1}	1e-14	5e-14	7e-15
Graphite exchange current	A/m^2	0.3	0.3	0.3
Maximum concentration	mol/m^3	30400	30400	11700
Reference concentration	mol/m^3	29640	16600	5850
Equilibrium potential	V	0.085	0.12	0.2

Table 5: Phase transformation parameters

Phase change properties	Unit	Value
Phase j to k rate constant, $k_{s,12}$ and $k_{s,23}$	$m^3/mol\text{-}s$	8.0e-8;1.5e-6
Phase j to k min limiting, $c_{s,1}^{*\min}, c_{s,2}^{*\min}$	mol/m^3	27300;13400
Phase j to k max limiting, $c_{s,3}^{*\max}, c_{s,2}^{*\max}$	mol/m^3	7300;17800

CHAPTER IV

THERMODYNAMICALLY CONSISTENT ANALYSIS ON POSITIVE ELECTRODES

Introduction

The first step towards creating a thermodynamically consistent approach in positive electrodes is to incorporate solid-state diffusivity change with SoC. Additionally, the equilibrium potential is made to be Nernstian in nature. The framework used has already been mentioned in Chapter III.

Thermodynamically consistent diffusivity

Firstly, the thermodynamically consistent solid-state diffusivity was first obtained and compared against a constant solid-state diffusivity. The solid-state diffusivity is taken to be average value of the varying diffusivity across the SoC.

Fitting the experimental OCP with Equation (17) using *nlinfit* function[85] on MATLAB and then using the coefficients mentioned in Table 6 in Equation (16), the thermodynamically consistent diffusivity is obtained as seen in Figure 6.

Table 6: Fitting Parameters for Nernst equilibrium potential

Phase	E^0	Ω_2/F	Ω_3/F	Ω_4/F	Ω_5/F	Ω_6/F	Ω_7/F	Ω_8/F	Ω_9/F
NCA	3.24	4.315	-0.3e2	1.5e2	-4.4e2	8e2	-8.3e2	4.5e2	-0.9e2

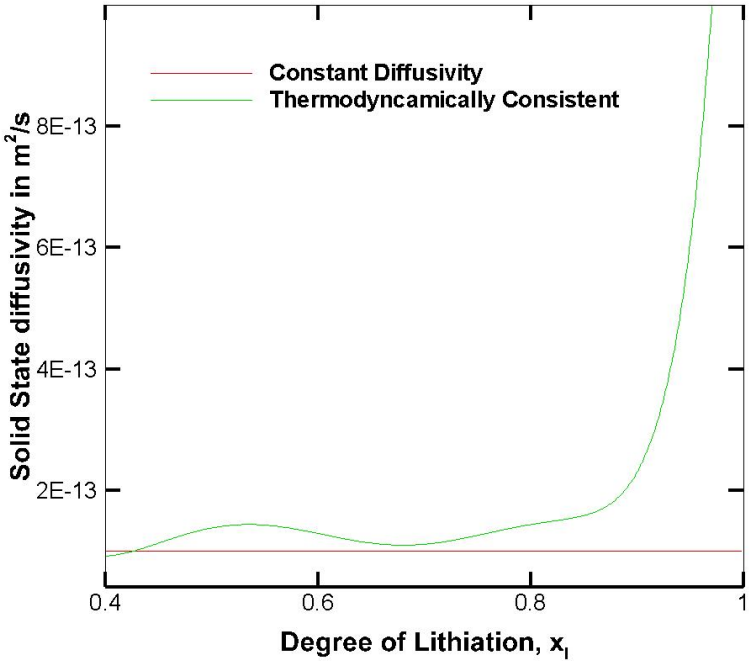

Figure 6: Thermodynamically consistent solid-state diffusivity vs constant diffusivity for NCAO electrode

Validation

The code was altered to a full cell code because the validation case used an NCA cathode and a graphite anode. The Fitted and assumed model parameters were obtained directly from Bernardi et al.[47]. The code ran successfully for a 40 second pulse, followed by a 160 second rest period for the re-equilibration of the system. The code for run for 5C, 10C and 20C as done in the paper and the results match closely to the results obtained by the author. The only difference is in the response time for the re-equilibration. The code that was developed by the Energy and Transport Science Lab (ETSL) at Texas A&M took

longer took a little longer as the solid-state diffusivity could not be reduced to the values considered by the Bernardi et al.

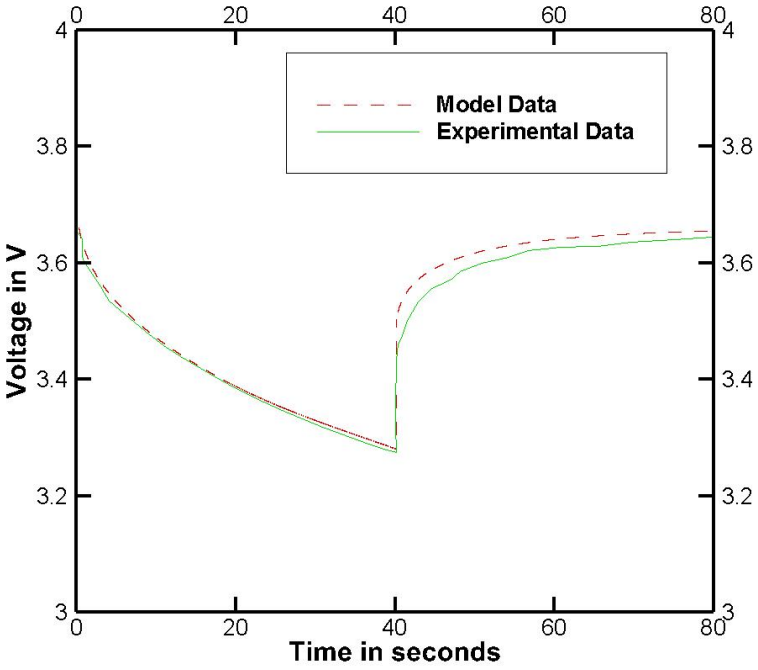

Figure 7: Plot comparing model results to experimental results of Bernardi et al. at 20C discharge pulse[41]

The parameters that went into the model came completely from Bernardi et al.[47] and there was nothing different except for the solid-state diffusivity value which was increased by a magnitude of 10 to prevent numerical instability from giving an accurate solution.

Once the solution was validated, it was then run to understand the effect of C-rate, electrode thickness and porosity on the performance of the half-cell with constant solid-state diffusivity and thermodynamically consistent solid-state diffusivity.

Effect of C-rate

The effect of C-rate on the performance of the electrode was looked at in this section by understanding the trends in Figures 8 through 11. C-rate is defined as the rate at which the battery is being discharged relative to its total capacity. A discharge of 1C implies that the battery takes about 1 hour to discharge. The time for discharge may reduce depending on the inherent ohmic losses in the cell. At low C-rates, very little difference between the thermodynamically consistent model and the constant diffusivity is seen due to low overpotential. As C-rate is increased, the constant diffusivity model starts to deviate at the end of the discharge cycle as compared to the TC model. This is because the diffusivity is higher in the TC model leading to better diffusion and a more lithiated electrode as compared to the constant diffusivity model which cannot make this prediction. As the C-rate is increased further to higher C-rates like 20C, a pronounced difference is seen between the two models. From Figure 7, it was evident that the thermodynamically consistent model matches experimental data at 20C meaning the capacity of the battery system under consideration is closer to experimental data. Thus, the importance of having a thermodynamically consistent model is seen at higher C-rates.

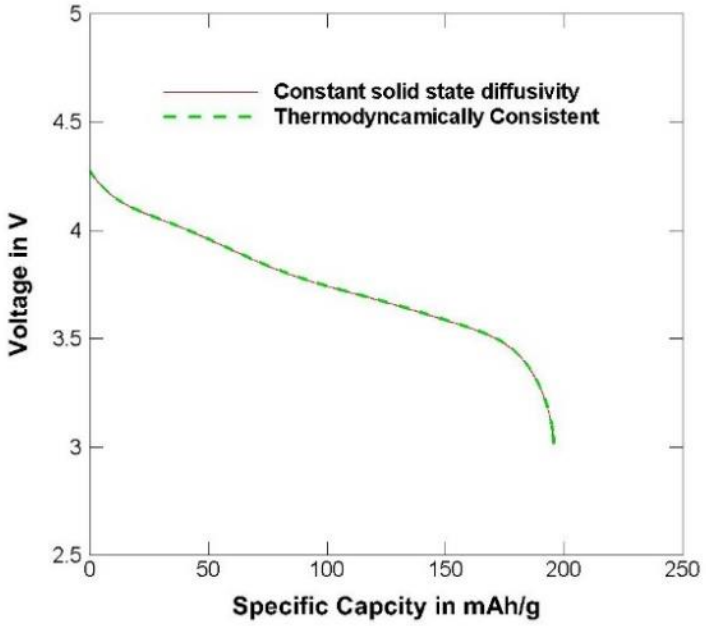

Figure 8: Discharge of NCA half-cell at 0.1C

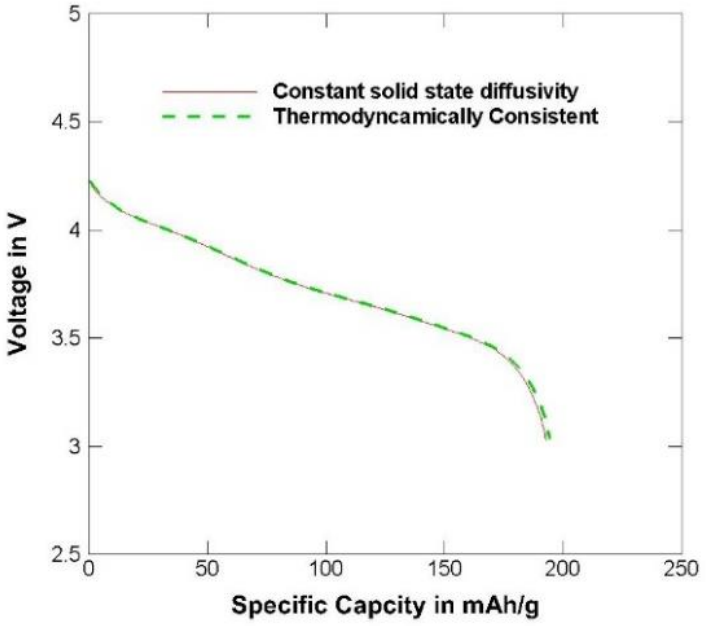

Figure 9: Discharge of NCA half-cell at 1C

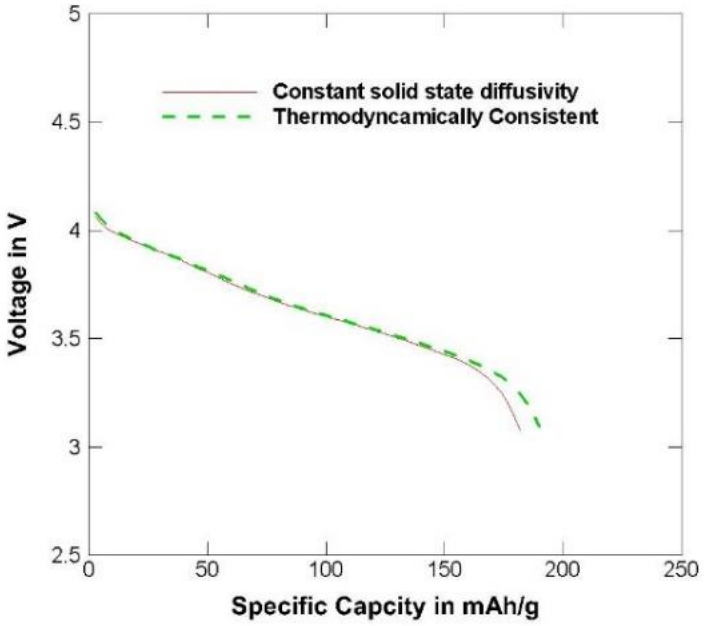

Figure 10: Discharge of NCA half-cell at 2C

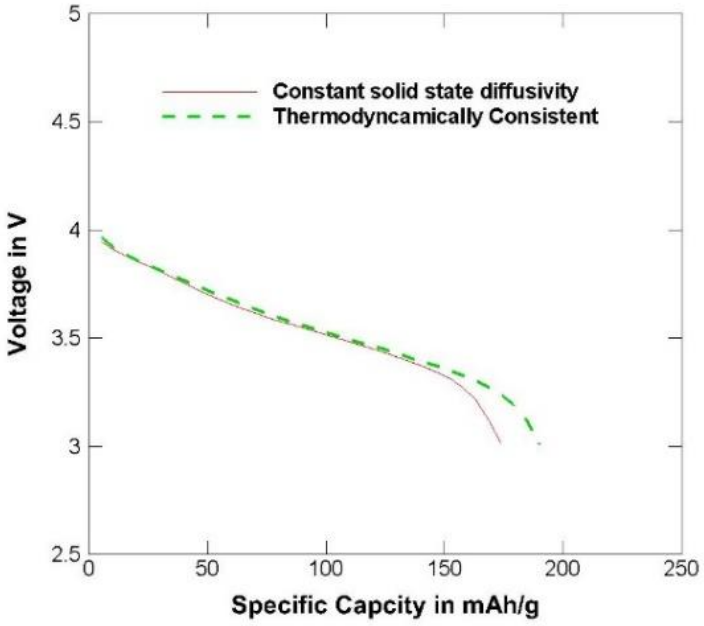

Figure 11: Discharge of NCA half-cell at 5C

Effect of electrode thickness

Increasing electrode thickness[86, 87] while retaining the porosity does two things: It increases the total amount of Lithium that can be shuttled and secondly, it increases the surface area over which the reaction can occur. The second factor is misleading since the increase of surface area also increases the volume. There is a particular value of electrode thickness beyond which the effects of the increased volume negate the increased surface area. Thus, increasing the surface area increases the amount of lithiation and thus a faster discharge time. Additionally, increasing the electrode thickness increases the transport losses that occur. This has not been captured in Figure 12 as the degeneration of electrolyte is considered minimal.

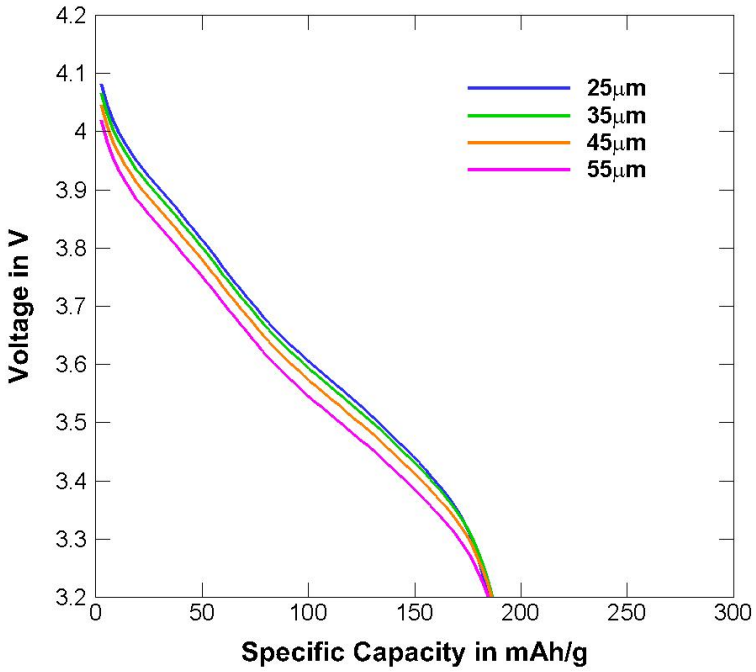

Figure 12: Effect of electrode thickness on NCA half-cell at 5C

Effect of particle size

Particle size is a measure of the average size of the conglomerate of particles that are present in the electrode. This is usually found using a scanning electron microscope. In this model, the particle size was looked at. Again, the particle size affects the surface area of the electrode intercalating[88]. Increasing the particle radius decreases the effective surface area (surface area/Volume) but the amount of lithium intercalating is the same thus not affecting the total capacity of the cell. Particle size of NCA electrode agglomerates are usually in the order of 5μm and this can be seen in Figure 13. The half-cell does not function as intended for particles that are larger than 8 μm.

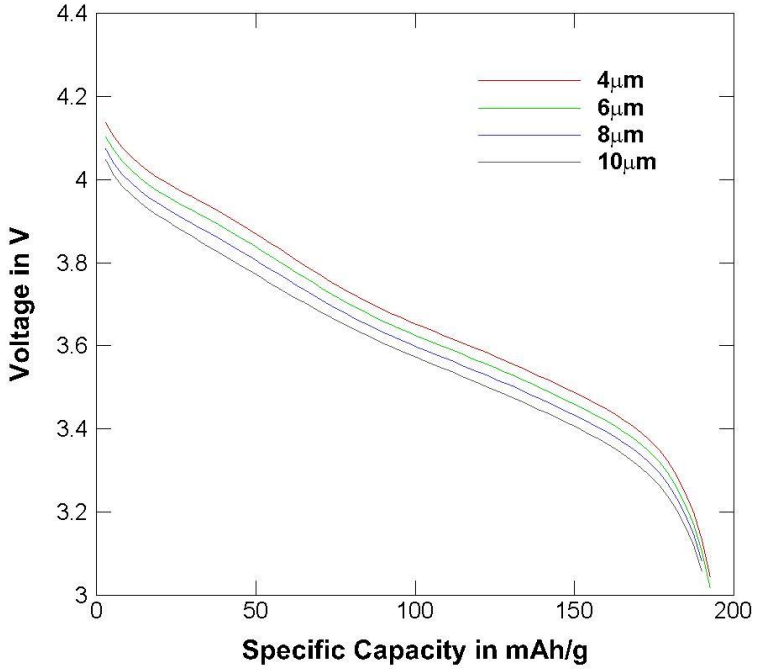

Figure 13: Effect of particle size on NCA half-cell at 5C discharge

Effect of active material

The effect of active material on the performance of the half-cell is complicated. If the active material fraction is increased, the amount of lithium present in the electrode is also increased but is being done so by reducing the amount of additives[89, 90] (binder, conductive additive). Also, the active material fraction has not increases b such a rate that it has affected the total capacity and the overpotential doesn't change too much by the increased lithium content. The increase of active material fraction and decrease of conductive additive have opposing effects leading to the performance remaining the same as seen in Figure 14.

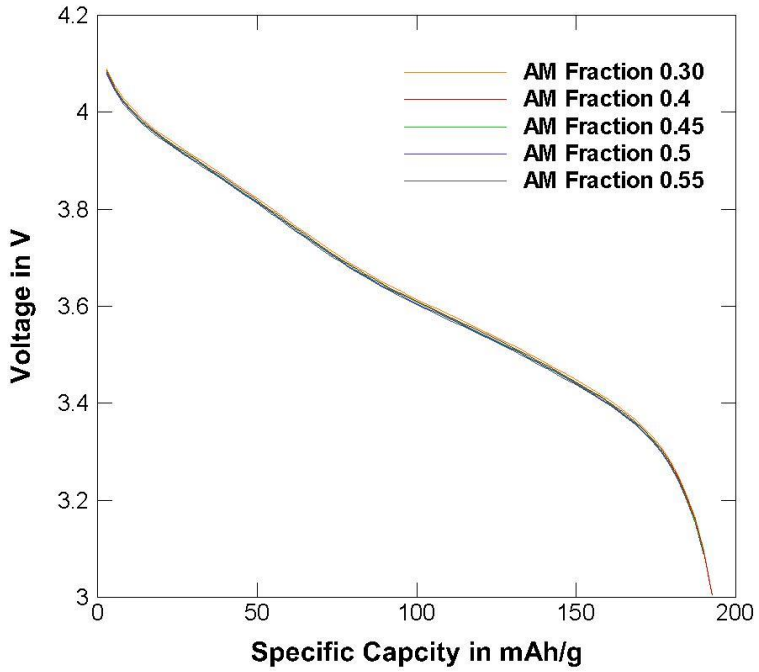

Figure 14: Effect of active material fraction on NCA half-cell performance at 5C

Conclusion

This concludes this chapter. The thermodynamically consistent solid-state diffusivity model has been validated and the effects of C-rate, electrode thickness, particle size and active material fraction on the performance of the half-cell has been understood. This code will now be extended to graphite to understand the effects on the physical parameters on the performance of the graphite half-cell incorporating phase transformation.

CHAPTER V

THERMODYNAMICALLY CONSISTENT ANALYSIS ON NEGATIVE ELECTRODES

Introduction

After successfully modelling a thermodynamically consistent model in a positive electrode, the concept is extended to electrodes with a plateau in its OCP profile. This, as discussed in earlier chapter implies a phase transition. Some positive electrodes have this plateau. A popular one is Lithium Iron Phosphate ($LiFePO_4$). In this study, graphite is of primary concern. It is widely used as an anode in Lithium-ion batteries. A lot of interest has gone into understanding the different phases of lithiated graphite[91-93] experimentally and theoretically. After considerable research, it can be said that 2 phases exist and have been found using in-situ experimental results[41]. Those phases are LiC_6 which has one Lithium intercalated in every sheet of the graphene structure and LiC_{12} which has 1 lithium particle intercalated in every second sheet of graphene. There is another plateau in the OCP profile of graphite but there has been quite a lot of debate as to the composition of it. In this study, it is taken to be LiC_{32}.

Thermodynamically consistent diffusivity

By extending the concepts used in the previous chapter, one can try to understand the thermodynamically consistent modelling of each phase of graphite. The first step towards doing this is to understand the open circuit potential of each phase of graphite.

In Bernardi et al.[38], U_{s1}, U_{s2} and U_{s3} represent the open circuit of the 3 phases i.e. LiC_6, LiC_{12} and LiC_{32}. From this point on, phase I corresponds to LiC_6, phase II corresponds to LiC_{12} and phase III corresponds to LiC_{32}. The OCP of each phase was fit against Equation (17) described in Chapter III. The fitting coefficients, found in Table 7 is obtained by fitting the OCP of each phase to the Equation (17). This can be inserted into Equation (16) to result in thermodynamically consistent solid-state diffusivity for each phase. The solid-state diffusivity vs state of lithiation is presented below for each state along with the constant solid-state diffusivity that is assumed in literature (Figures 15-17).

Table 7: Thermodynamically consistent fitting parameters for the 3 graphite phases

Phase	E^0	Ω_2/F	Ω_3/F	Ω_4/F	Ω_5/F	Ω_6/F	Ω_7/F	Ω_8/F	Ω_9/F
LiC_6	0.085	0.343	-1.31	1.77	2.9594	-13.92	20.046	-13.24	3.39
LiC_{12}	0.12	-0.796	4.382	-12.95	24.00	-28.74	21.801	-9.626	1.899
LiC_{32}	0.3	-1.2e3	6.47e3	-1.7e4	2.7e4	-2.7e4	1.63e4	-5.6e3	846.7

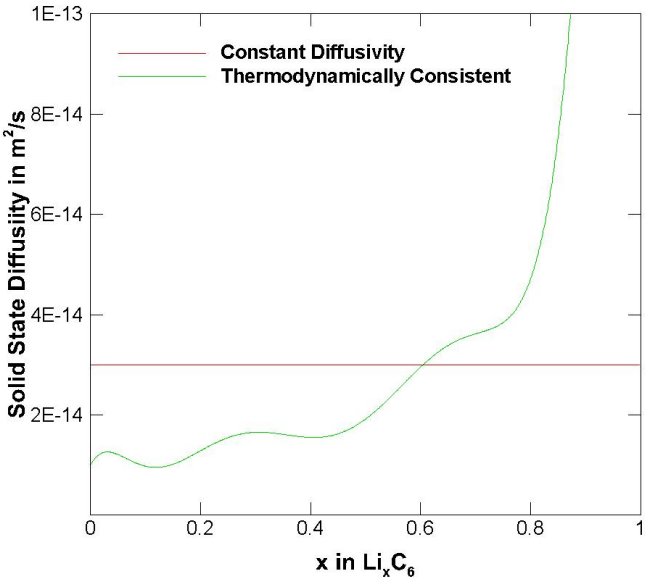

Figure 15: Constant vs TC solid-state diffusivity for LiC_6

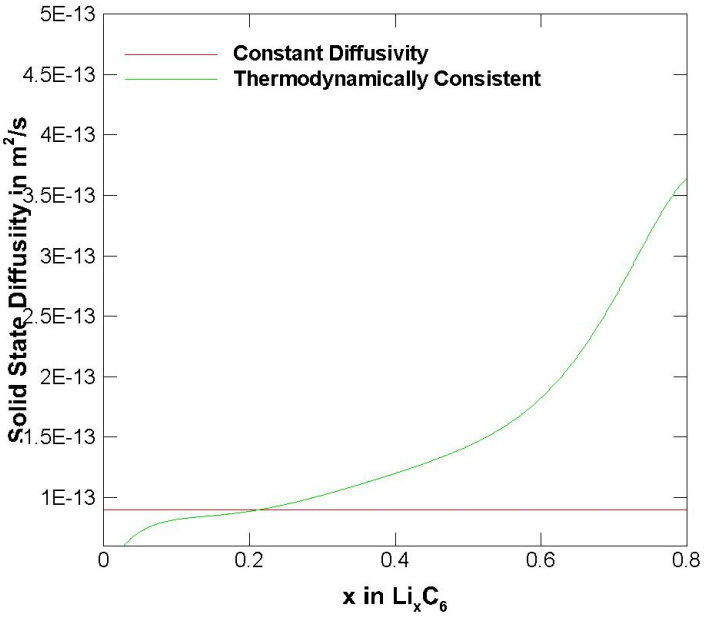

Figure 16: Constant vs TC solid-state diffusivity for LiC12

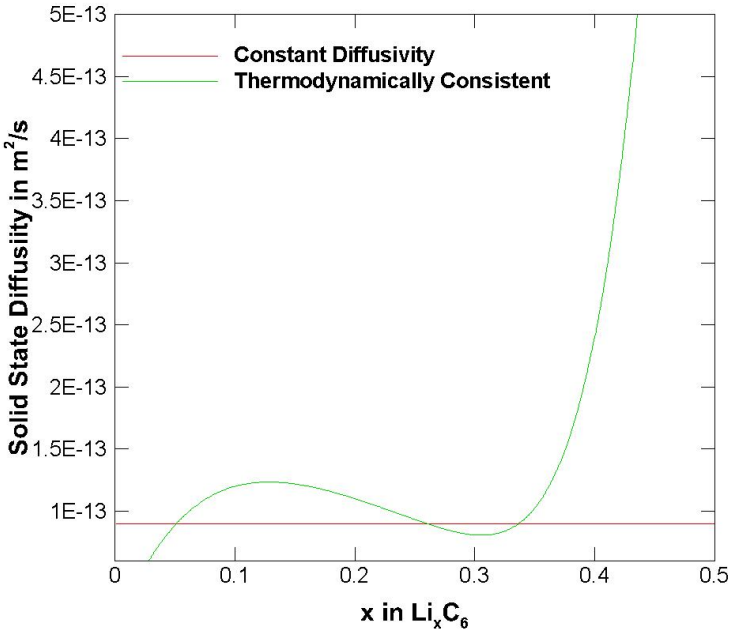

Figure 17: Constant vs TC solid-state diffusivity for LiC_{32}

Validation

Phase change was incorporated into the half-cell. Since the formulation for the phase change was quite complicated and involved the introduction of numerous new variables, the code had to be re-validated with data provided by Gallagher et al.[46]. The only difference in data as compared to what was published in the paper was the solid-state diffusivity values, which were constant for validation purposes. The code was validated for C/10 and phase transformation was captured. The results in Figure 18 and Figure 19 show the good fit between results published and the model created for this study.

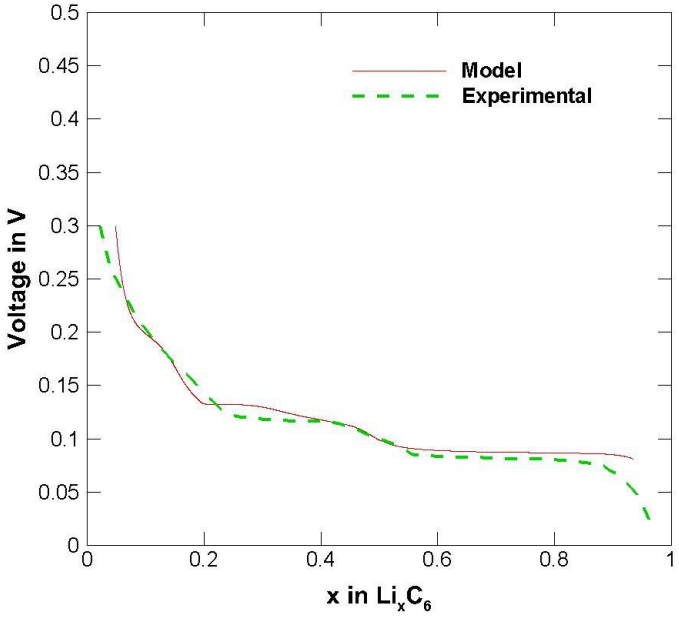

Figure 18: C/20 experimental data vs model for graphite half-cell

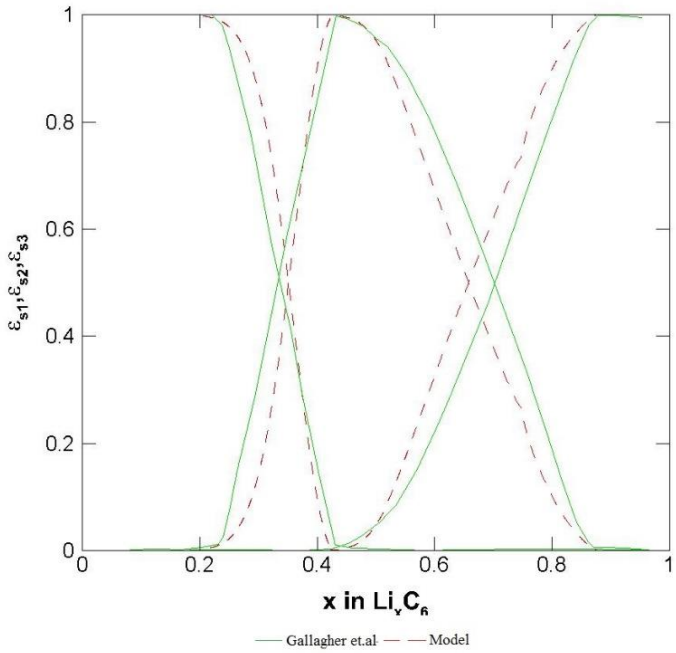

Figure 19: Gallagher et al. phase change vs current model at C/20

Effect of C-rate

C-rate is a measure of the rate at which the battery discharges/charges as mentioned in the previous chapter. C-rate has the effect of increasing the current density at which, in this case the graphite electrode lithiates. It also affects the phase transformation behavior. There are two aspects to this study. The first is to understand the difference between constant solid-state diffusivity and thermodynamically consistent solid-state diffusivity (Figures 20-23. The second aspect to understand how C-rate affects phase transformation (Figures 24-27).

In the validation case, the phase transformation at slow kinetics conditions can be seen. Ideally, all the LiC_6 transforms to LiC_{12} which then completely transforms into LiC_{32}. As C-rate increases, the rate of transformation from LiC_6 to LiC_{12} to LiC_{32} reduces. This is because the kinetics of phase transition is much lower than the rate at which particles are being intercalated.

As C-rate is increased, the highly intercalated regions have better solid-state diffusivity due to bulk movement of the lithium ions in the electrode. This is the premise of the thermodynamically consistent model. This can be seen at high C-rates. At low C-rates, the overpotential created is lower meaning there would be no significant difference between the thermodynamically consistent model and the constant diffusivity model. Like in the NCA positive electrode, as the C-rate is increased, a difference starts to emerge between the two models.

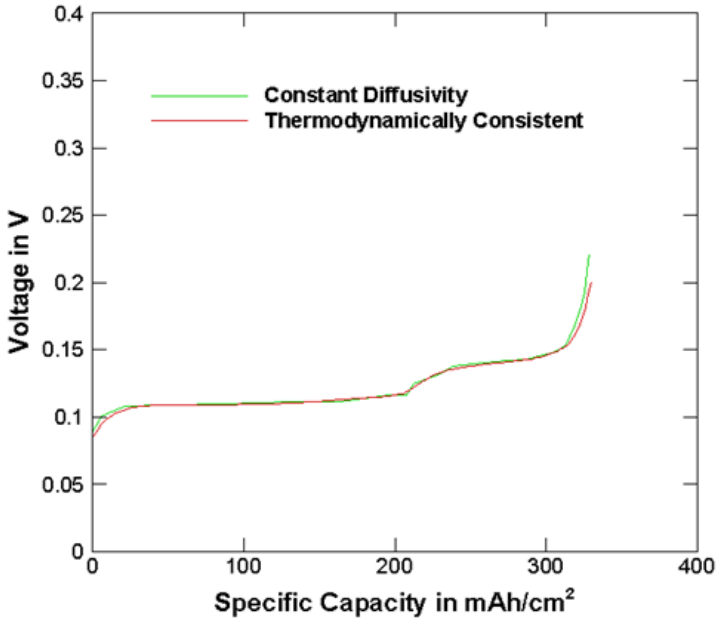

Figure 20: C/4 de-intercalation of graphite half-cell

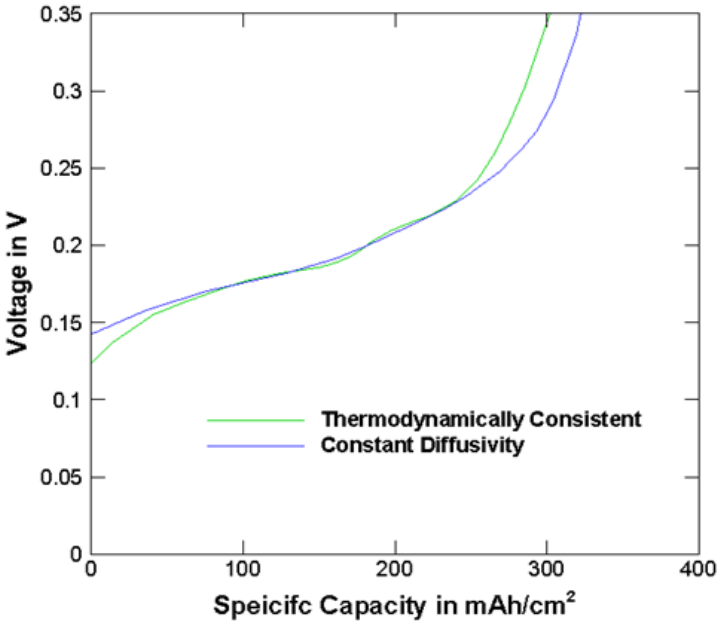

Figure 21: 1.25C de-intercalation of graphite half-cell

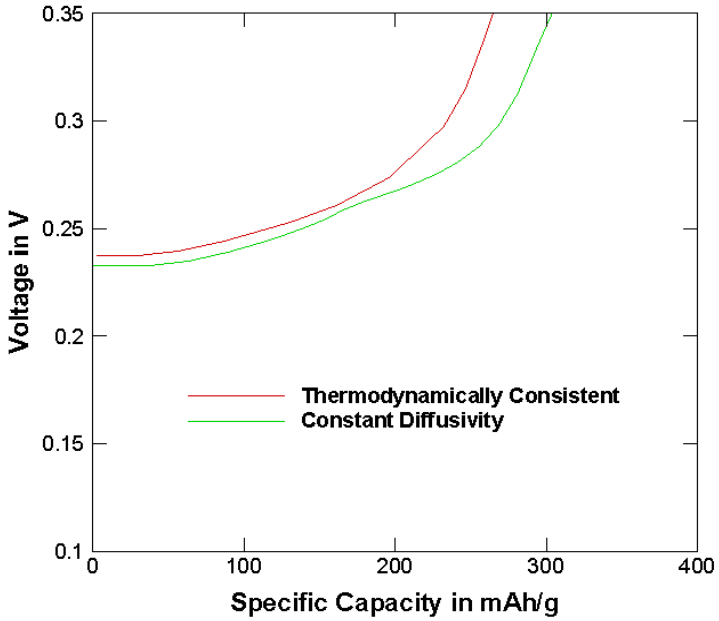

Figure 22: 2.5C de-intercalation of graphite half-cell

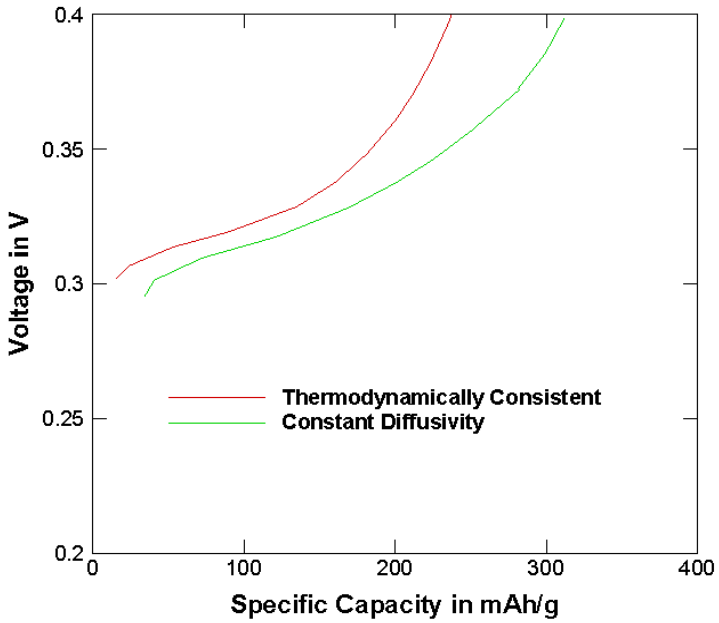

Figure 23: 5C de-intercalation of graphite half-cell

The next section goes into how phase transformation is affected by C-rate (Figures 24-27). As the C-rate is increased, the overpotential created between the electrode and electrolyte increases. In the thermodynamically consistent model, this ensures smoother movement of lithium ions and a smaller gradient between the surface of the particle and the interior, especially at high stages of lithiation. As de-lithiation begins, the thermodynamically consistent model, the lithium is being shuttled across the radial shell and since the SoC is a function of the surface concentration, it appears to have higher volume fraction at any given moment. Also, during the transition from phase I to phase II, having lower diffusivity ensures that the phase change occurs at a more de-lithiated state because in the current model, the super-saturated zone at which phase transformation occurs is a function of concentration of each of the species. Also, a thermodynamically consistent approach better predicts the volume fraction of each phase more accurately if the voltage profile is fitted to experimental data as it represents accurate physics.

The surprising find was that as the C-rate was increased, the difference between the phase transformation behavior using the thermodynamically consistent model and the constant diffusivity model is lesser. This could be because of the difference in the kinetics between phase transformation and intercalation. The intercalation happens so quickly that the phase transformation is forced rather than induced due to favorable concentration conditions.

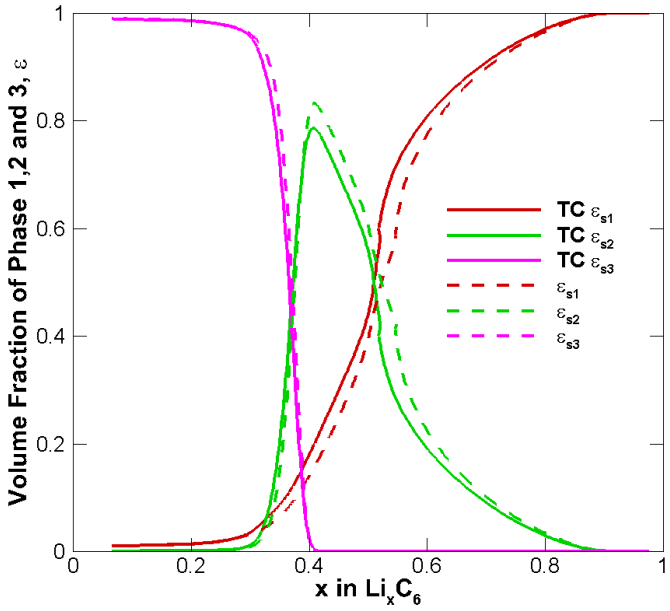

Figure 24: TC diffusivity vs constant diffusivity for 0.25C

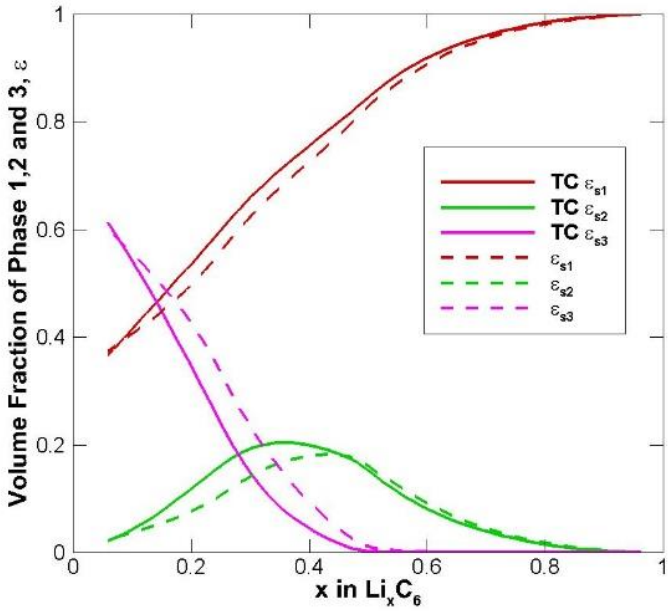

Figure 25: TC diffusivity vs constant diffusivity for 1.25C

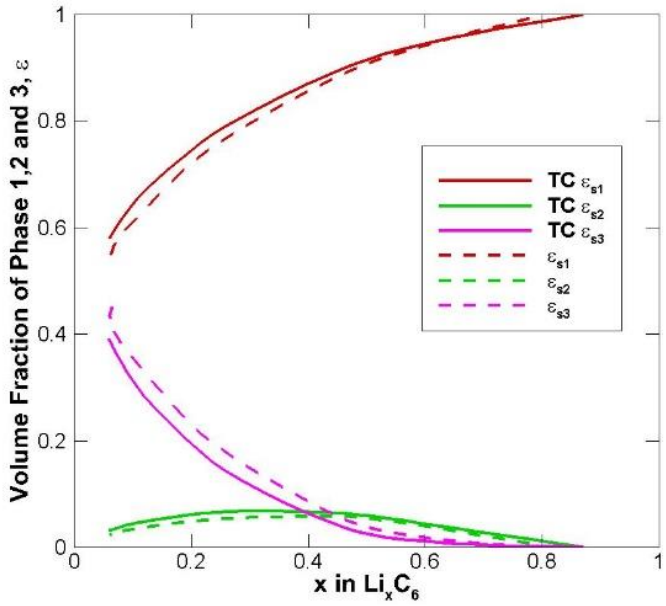

Figure 26: TC diffusivity vs constant diffusivity for 2.5C

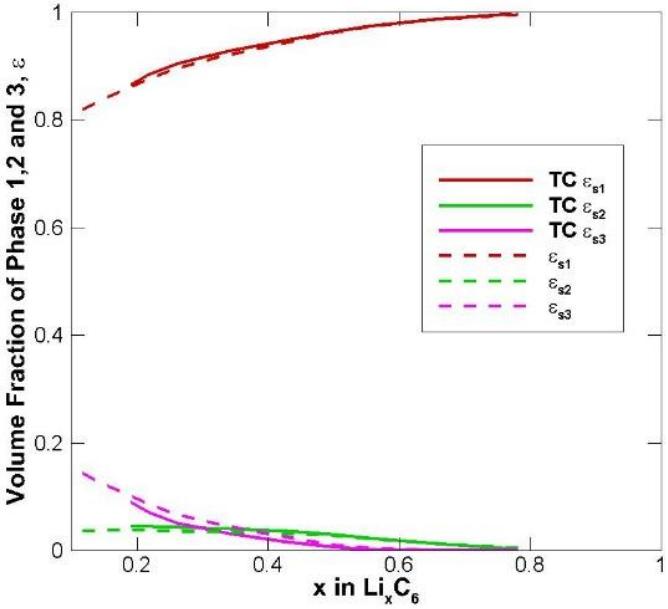

Figure 27: TC diffusivity vs constant diffusivity for 5C

Effect of electrode thickness

The effect of electrode thickness on the electrode was discussed in the previous chapter and the reasoning would be the same for the graphite electrode as well. Increasing the electrode thickness without increase of porosity increases the surface area available for intercalation. Thus, increase in the electrode thickness would increase the rate of de-intercalation or intercalation. Increasing the electrode thickness primarily increases the ohmic resistance that the lithium ion faces during intercalation or de-intercalation. This increases as the thickness is increases as seen in Figure 28.

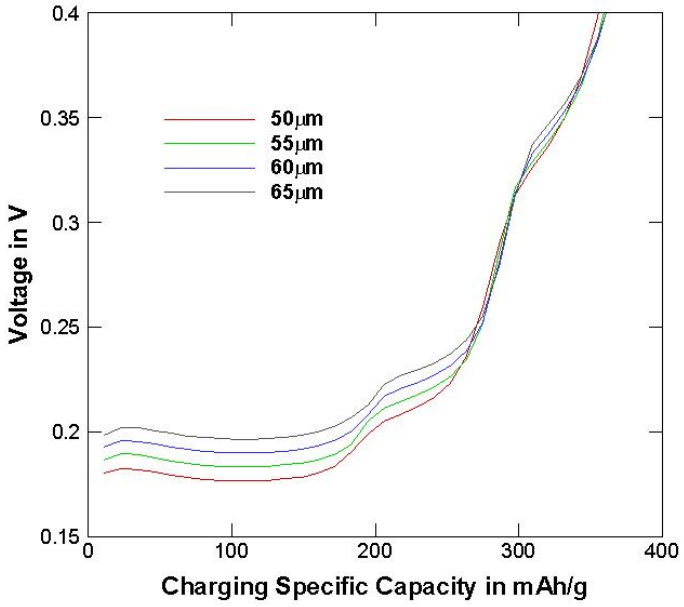

Figure 28: Effect of electrode thickness at 1.25C

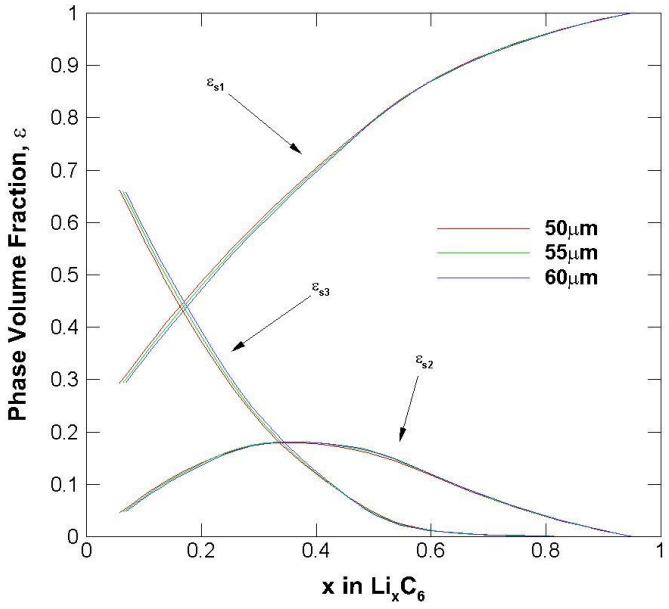

Figure 29: Effect of electrode thickness on phase transformation at 1.25C

Regarding phase transformation of graphite, as the electrode thickness is increased, the surface area increases which increases the rate of removal of the lithium ions. Thus, phase I starts reducing at a faster rate with the 55μm electrode which in turn increases phase II. The same trend can be observed for the phase II to phase III transformation in Figure 29.

Effect of particle size

Particle size is the size of the particle agglomerate in the electrode. Positive electrodes are usually smaller at around 5μm whereas graphite generally forms more agglomerates and is usually 10μm in size. Changing the particle size has the same effect as increasing the electrode thickness. It increases surface area but does not change the

amount of lithium present. Hence, the total capacity would not change by a large extent but it should be noticed that the larger size leads to faster de-intercalation. Increase in the radius decreases the specific area as the volume increases with increase in radius faster than the surface area does. In Figure 30 below, these features can be noticed. The code is sensitive to the specific surface area of the phase which directly affects the current density of each phase. It was noticed this especially with the reduction of the radius of the particle to a value below 10μm. This seemed to affect the results by a greater manner than expected (Figure 31). Hence, the study was careful not to reduce the radius of the particle below 9μm.

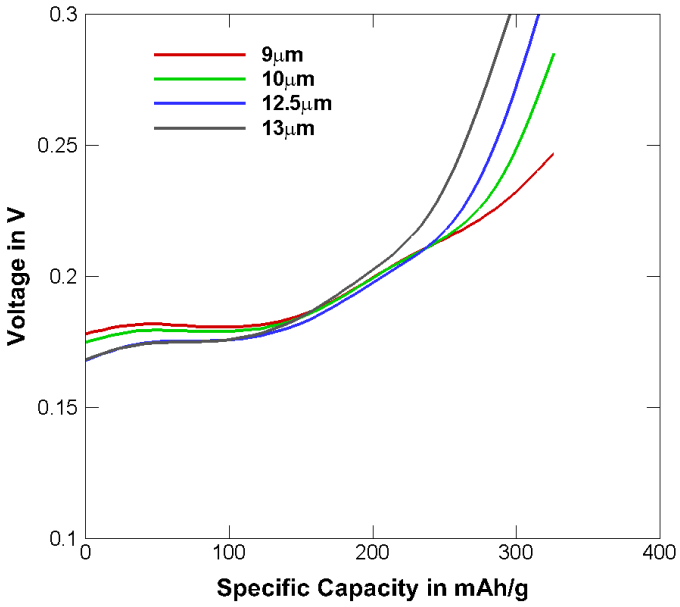

Figure 30: Effect of particle size at 1.25C

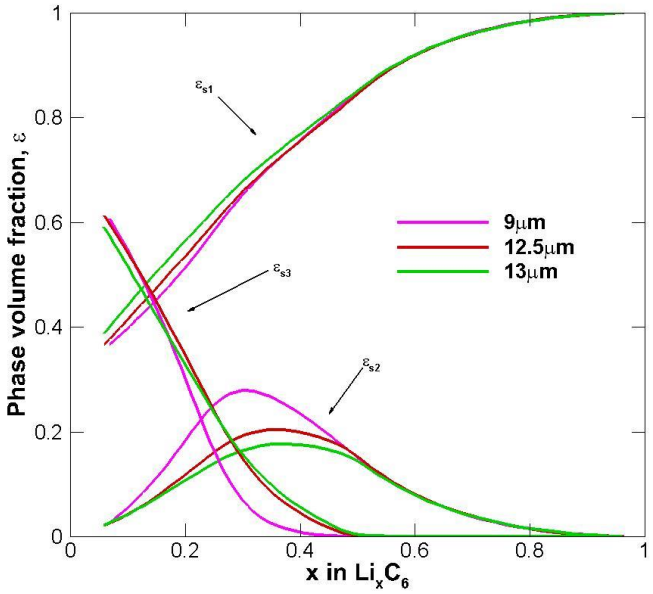

Figure 31: Effect of particle size on phase transformation at 1.25C

Effect of active material

Unlike in the positive electrode, the negative electrode does not need a conductive additive. This is because the electrode is already made of graphite which has a high electrical conductivity. Thus, increasing the active material increases the amount of Lithium with no counter effect of reducing conductive additives. Thus, increasing the active material increases the amount of lithium in the electrode and thus leads to increased overpotential and faster de-intercalation. Another way of looking at it is that the electrochemical flux is reduced with increase in active material. This is seen in the Voltage vs specific capacity profile. Found below are Figures 32 and 33 that help understand graphite voltage and phase transformation curves at various active material fractions of 0.4, 0.45, 0.5, 0.55 and 0.6.

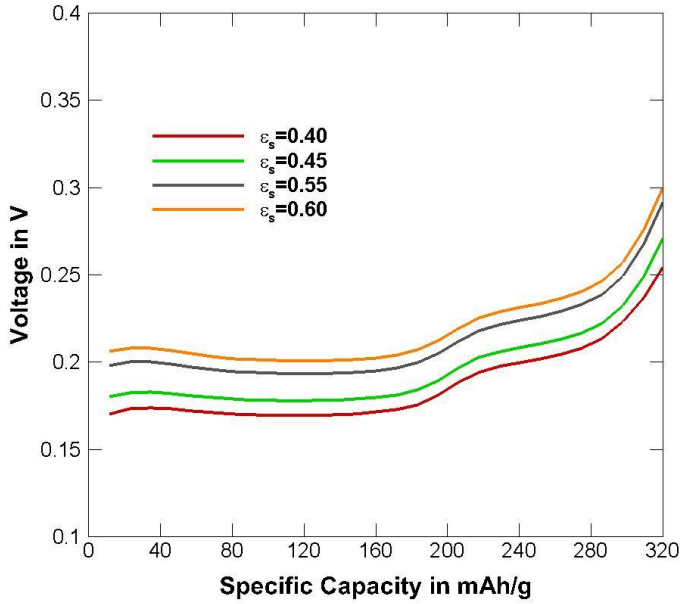

Figure 32: Effect of active material at 1.25C

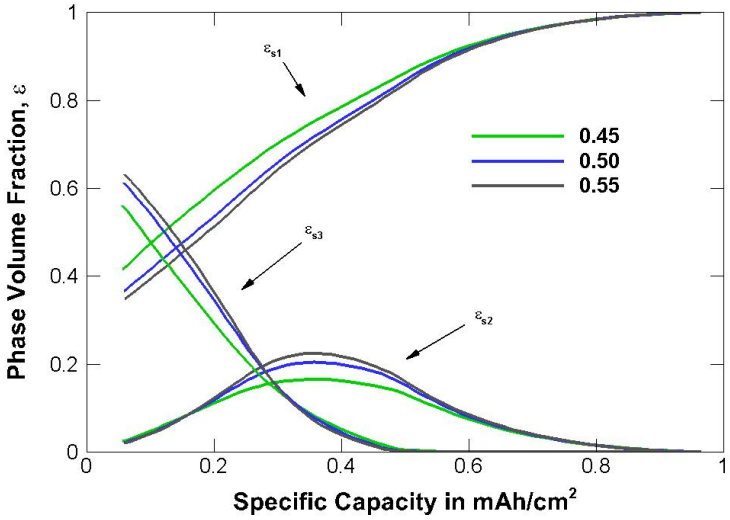

Figure 33: Effect of active material on phase transformation at 1.25C

With phase transformation, the trigger for nucleation is concentration. Thus, with higher active material fraction, phase 2 has the highest peak in the highest active material

region because the flux density is the lowest. This would imply that it would take longer to phase transform but would also imply that the SoC reduces at a smaller rate. This can be seen more clearly in the volume fraction vs specific capacity plot (Figure 34) below.

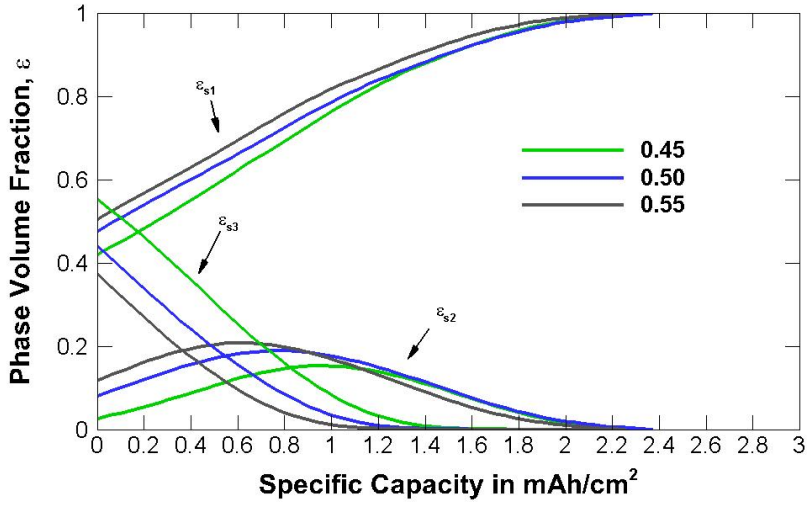

Figure 34: Phase transformation vs specific capacity at 22 A/m^2

Visualization of phase change

Phase change was captured but to visualize the phase change occurring, a model was created through which phase change through the particle is visualized through a series of images. The color bar on the right-hand side of each image gives a representation of the average volume fraction in the region.

In Figure 35 seen below, from left to right and then to the left most column of the next row and so on, LiC_6 during de-intercalation undergoes constant de-intercalation as it nucleates to form LiC_{12}. This is concentration dependent and hence the first slide can be noted to be completely LiC_6.

Visualization of LiC_6

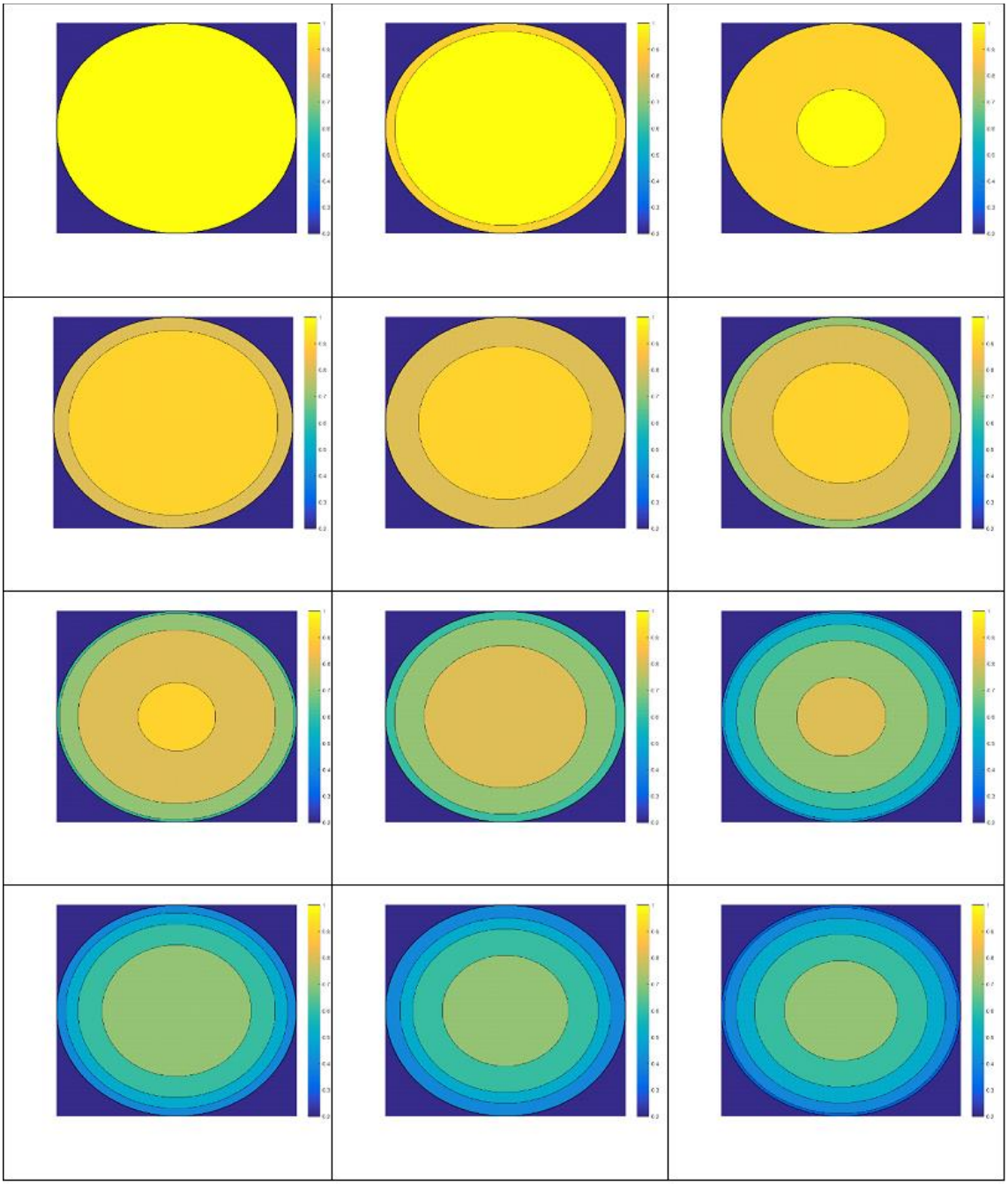

Figure 35: Visualization of phase change in LiC_6

Visualization of LiC_{12}

Unlike LiC_6 which constantly de-intercalates, LiC_{12} first intercalates as LiC_6 nucleates and then starts to nucleate to form LiC_{32}. The nucleation is based on concentration of the particles at the surface. This can quite clearly be observed in Figure 36 as the color changes from blue (lower concentration) to yellow (higher concentration).

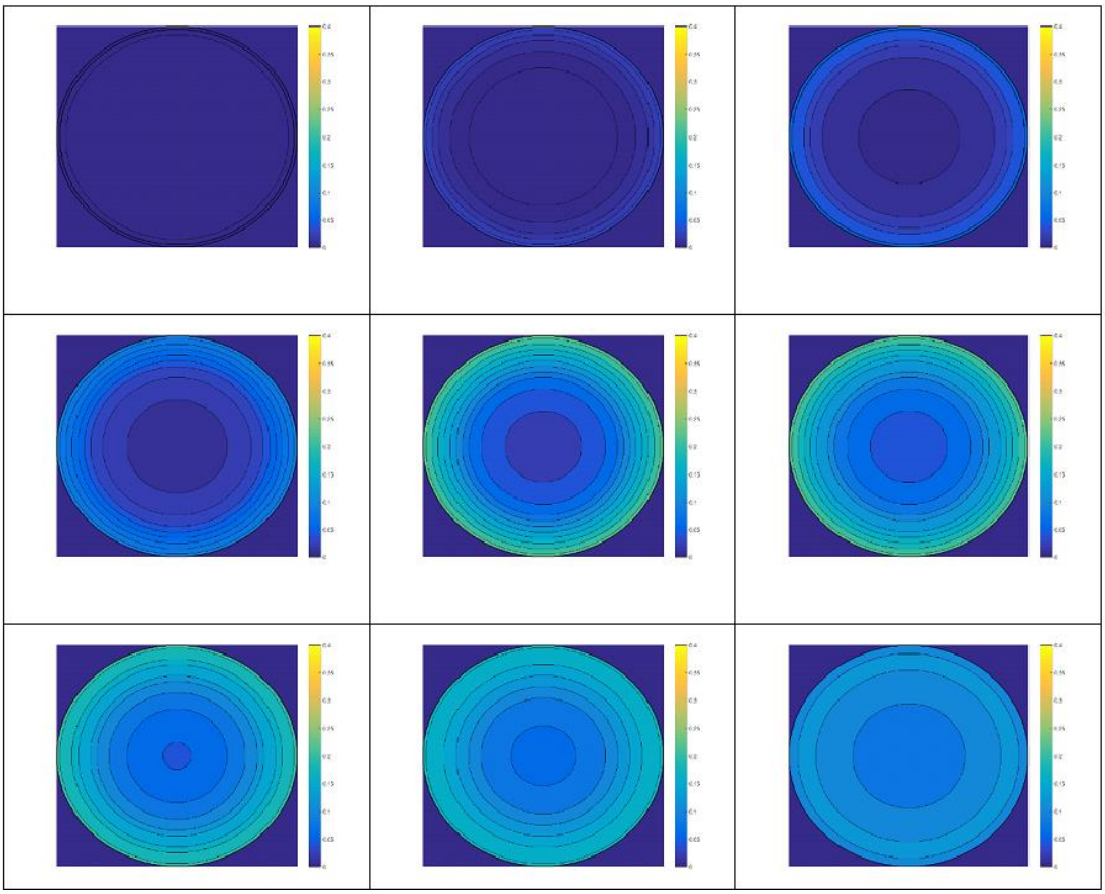

Figure 36: Visualization of phase change in LiC_{12}

Visualization of LiC_{32}

LiC_{32} only increases in volume fraction as LiC_{12} nucleates to create LiC_{32} in the electrode. This is seen increasing from the surface with solid state diffusion dictating the speed at which the volume fraction is seen throughout the particle.

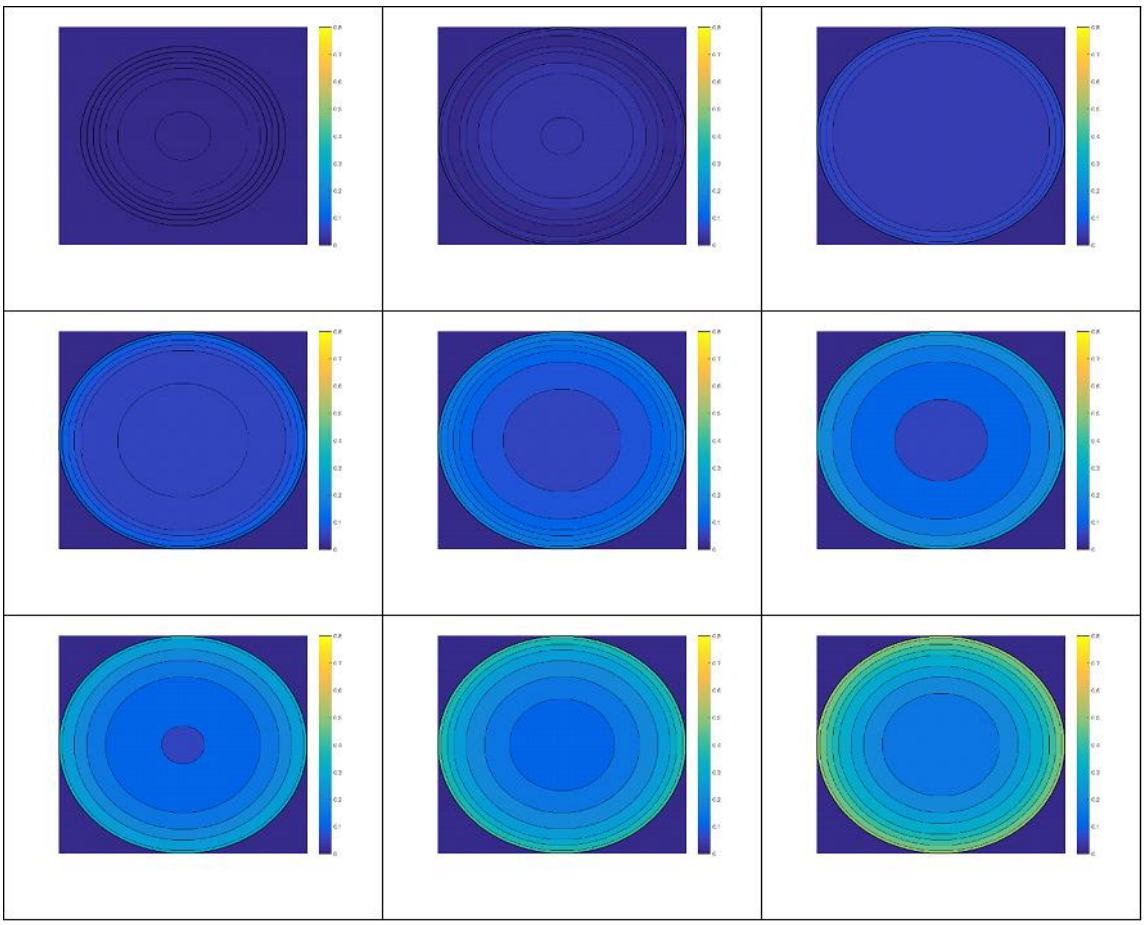

Figure 37: Visualization of phase change in LiC_{32}

As with thermodynamically consistent modelling, the phase change is seen to increase uniformly throughout the particle at the earlier stages and only at later stages do

you see significant difference between the surface shell and the inner shells of the electrode particle. This trend is quite evident in Figure 37.

Conclusion

The graphite half-cell model has been verified to a graphite electrode while accounting for phase change. The code shows that at low C-rate discharge, multiple plateaus in the voltage profile are observed that correspond to the phase change of LiC6 → LiC12 → LiC32. The change of the different phase is also elucidated. The effect of C-rate, electrode thickness, porosity, active material fraction is shown in this chapter. The code in this form is extremely computationally intensive and has only been validated for discharging conditions. The same code cannot be easily reversed due to numerical difficulties that can only be overcome by making non-physical reasoning. Hence, a graphite C++ code was created which does not account for phase change. This code does account for thermodynamically consistent behavior. It will be extended to incorporate Lithium plating at different environmental temperatures and C-rates to understand how a more accurate model can better predict lithium plating in a graphite half-cell.

CHAPTER VI

THERMODYNAMICALLY CONSISTENT ANALYSIS ON NEGATIVE ELECTRODES WITH LITHIUM PLATING

Introduction

Lithium plating has been a major issue for Lithium ion batteries for a long time now. It has been extremely hard to experimentally find lithium plating in graphite electrodes using non-destructive methods. Only recently have studies been done that have captured trends of lithium plating at different temperatures and C-rates. It would be extremely beneficial to a model that could first and foremost validate lithium plating and then extend the same concept further. A thermodynamically consistent approach would suggest that at higher states of lithiation, the diffusivity of the electrode is better which would imply that transport within the electrode improves. This would suggest that the lithium plating that occurs on the electrodes are not as bad as the models are currently predicting. Better transport within the solid state leads to lower overpotential created at the surface and hence, lower lithium getting plated on the surface. The following chapter tries to understand the behavior of lithium plating at low temperatures and high C-rates.

The voltage of the half-cell is plotted below at the two extreme temperature conditions observed in the study. Lithium ions work best at 298 ± 20 K. Any further deviation from these temperatures result in reduced capacity utilization, as seen in Figure 38. Most of this performance difference should do with low solid-state diffusivity and increased transport losses. This can be observed in the plot below. As temperature drops,

the electrode properties[94, 95] and electrolyte properties that are affected by temperature also reduce. This in turn manifests itself in the reduction of the solid-state and electrolyte potentials which can be seen in the profile below as a drop in voltage vs time/specific capacity.

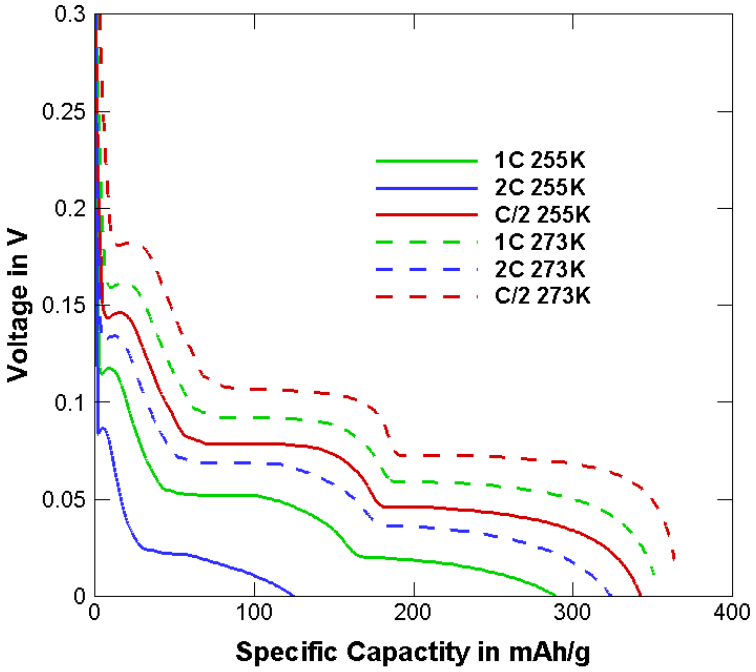

Figure 38: Voltage vs specific capacity for graphite half-cell at 255K and 273K

Effect of temperature on Lithium plating

In this section, the effect temperature on lithium plating is understood with the help of Figures 39-41. Lithium plating occurs when the solid-state potential is lower than the electrolyte potential. As the temperature reduces, the electrode and electrolyte properties drop according to the Arrhenius relation for temperature. This relation is

exponential in nature. Thus, the initial drop in temperature from 293K is the most significant in terms of the property change. From 293K to 273K, there is hardly any difference in the performance but as the temperature is reduced, the properties such as rate constant for intercalation, solid state diffusivity, electrolyte diffusivity and ionic conductivity in the electrolyte phase fall off quite significantly causing the solid-state potential and electrolyte potential to drop. This is reflected in the lower voltage profile at lower temperatures. Thus, as temperature is decreased, lithium plating increases. There is no lithium plating observed until 273K because there is no degradation in electrolyte and electrode properties until this temperature.

As the ambient temperature drops, the SoC at which lithium plating is initiated also changes. In other words, the amount of lithium shuttled into the electrode from the electrolyte is different. This in turn affects the performance of the half-cell.

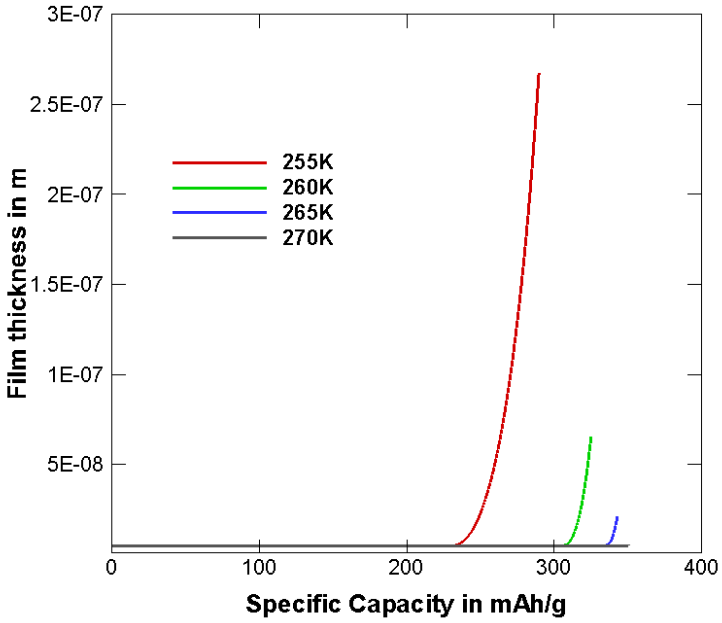

Figure 39: Lithium plating film thickness in m vs specific capacity at 1C

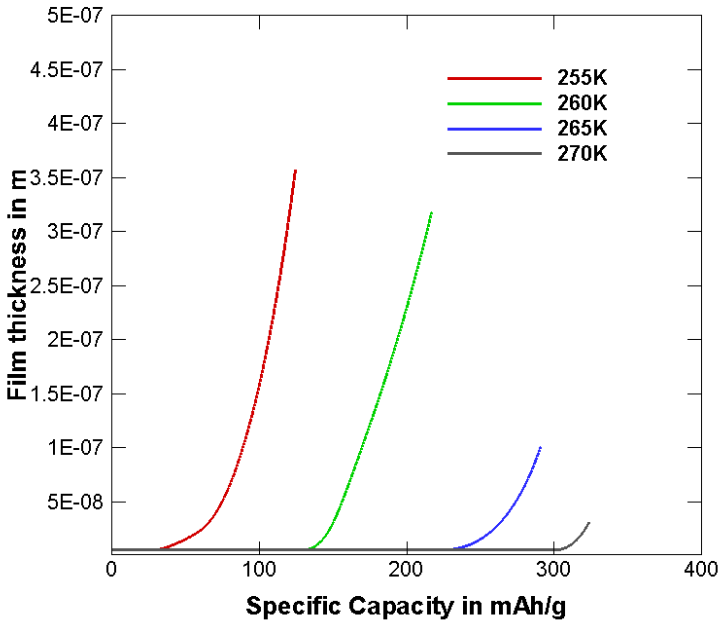

Figure 40: Lithium plating film thickness in m vs specific capacity at 2C

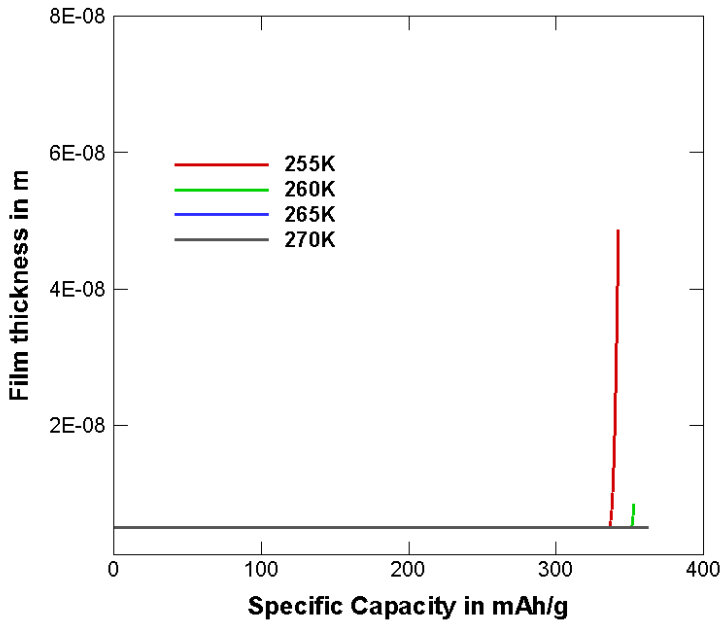

Figure 41: Lithium plating film thickness in m vs specific capacity at 0.5C

From the three plots above, the higher the C-rate, the more is the lithium plating that occurs but more attention is given to that in the next section. As temperature is decreased from 270K to 250K, one can notice that the amount of lithium plating for any C-rate condition increases. Decreasing the temperature leads to electrode properties becoming worse. The solid-state diffusivity and lithium transport are affected greatly. This leads to an overpotential being created at the surface of the electrode which starts to build up. This overpotential creates a condition where lithium ions can no longer be lithiated and is forced to instead precipitate or coat the surface of the electrode. This increases the resistance of flow further as lithium metal is now covering the pores through which particles would normally diffuse. In most of the cases above, at 270K, plating does not

start. This is because the electrode and electrolyte properties are not affected greatly until this temperature. Going lower causes lithium plating to occur. The film formation is exponential because lithium plating further causes more plating to occur.

Effect of C-rate on Lithium plating

The effect of C-rate on a graphite half-cell was discussed in the previous chapters. Increasing C-rate increases the current density that is being applied. In other words, the potential that is created to either pull the lithium ions from the electrode or to insert them into the electrode from the electrolyte increases. The effect of C-rate alone is enough to cause lithium plating, as can be seen in Figures 42-45. Plating is observed at high C-rates even at relatively high temperatures of 273K. This overpotential at low temperature is highly negative which leads to lithium metal being pushed into the electrode a rate faster than the solid-state diffusion can handle.

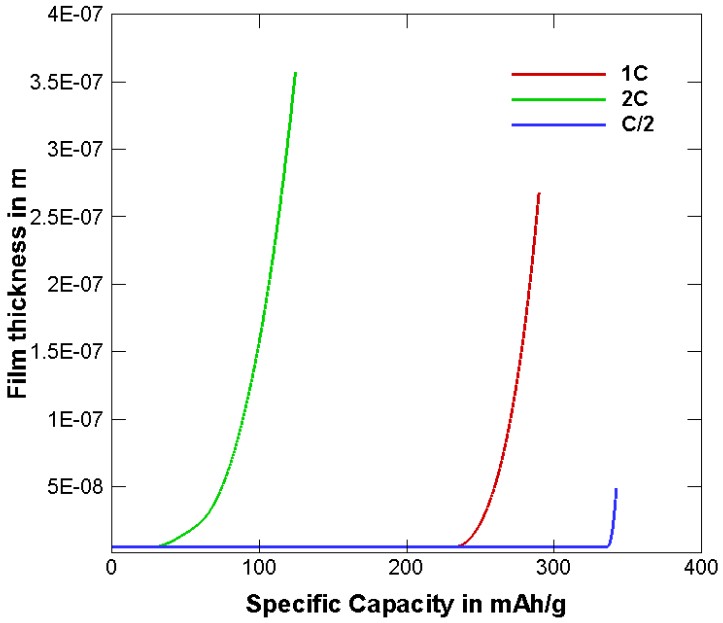

Figure 42: Film thickness vs specific capacity at 255K

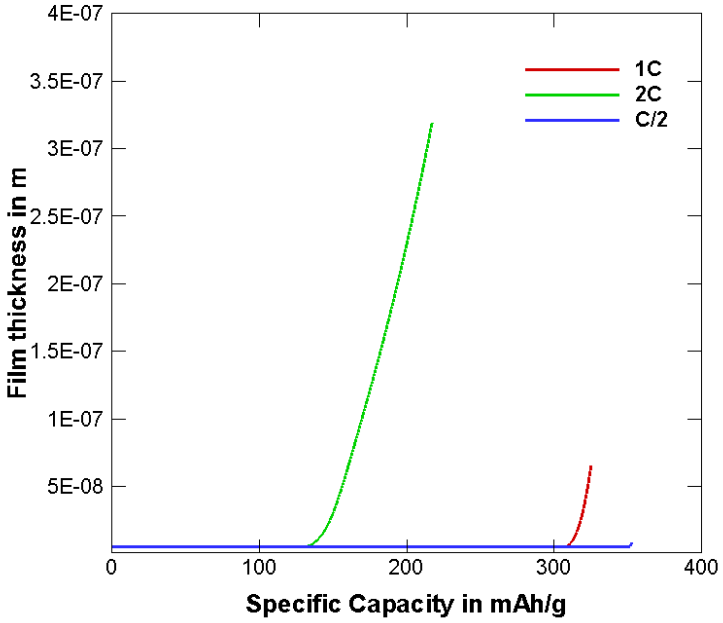

Figure 43: Film thickness vs specific capacity at 260K

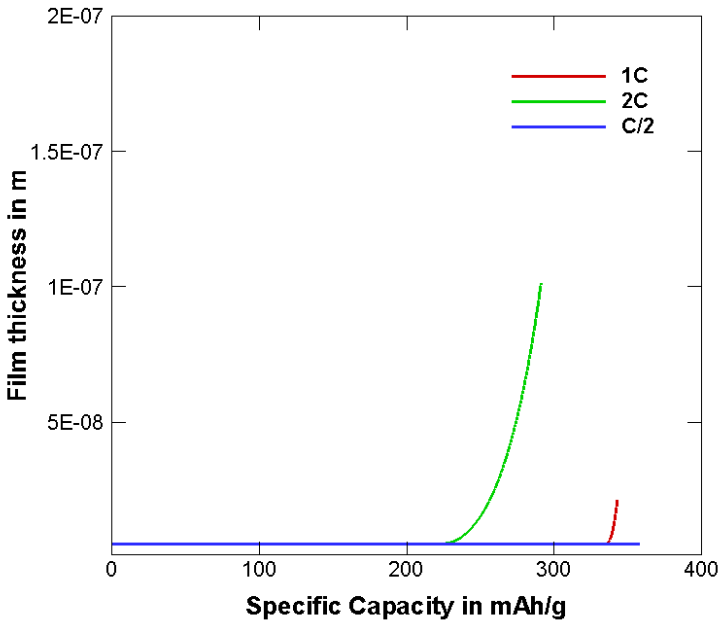

Figure 44: Film thickness vs specific capacity at 265K

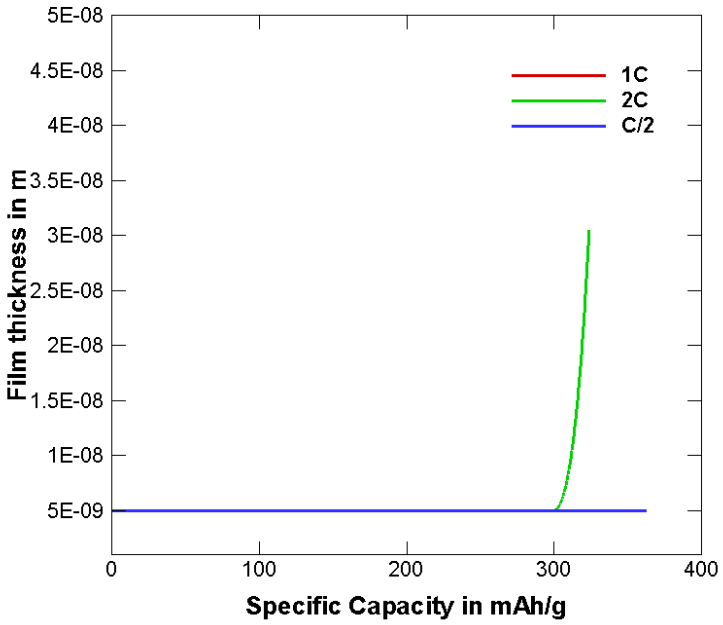

Figure 45: Film thickness vs specific capacity at 270K

When this overpotential causes the electrolyte potential to become higher than the solid-state potential, lithium plating occurs. As the C-rate increases, this overpotential only increases. C-rate has as big as impact on the lithium plating as temperature. This has not been of as much focus as temperature has had in earlier works[39, 70, 75].

From the plots above, it can be noted that lithium plating is generally higher for higher C-rates. As temperature reduces, the thickness of the lithium plating film only increases and does so at an exponential rate. Thus, creating low temperature situations for high C-rate applications is generally very dangerous for the performance of the Lithium-ion system. Another important observation is that with the increase in the lithium plating, the specific capacity of the battery system reduces. This is because lithium plating causes the lithium ions which would generally lithiate and provide electrons for the generation of electricity are now being plated on the surface of the electrode. This is an irreversible reaction and leads to a loss in the total lithium that can lithiate. This corresponds to a loss in capacity. Also, lithium plating causes the surface area to reduce. This can make lithium ions that are present difficult to reach or conversely, during charge, pores hard to access. This will further reduce the total capacity of the electrode.

Effect of electrode thickness on Lithium plating

The effect of electrode thickness on a graphite half-cell at normal temperature conditions has already been discussed in the previous chapter. Increasing the electrode thickness increases the amount of lithium available for intercalation and thus the total

capacity of the electrode. The increase in the electrode thickness also increases the current density that is correlated to 1C discharge. 1C current is the current density that is required to discharge or charge the electrode in 1 hour. If more lithium is now present as a result of the electrode thickness increase, it corresponds to increase in the current density as well. From previous sections of this chapter, it was noted that increase in C-rate and lowering of temperature affect lithium plating. The increase in electrode thickness increases the total amount of lithium that can intercalate but that is also available for lithium plating. A larger current density leads to a larger overpotential and results in lithium plating to occur. Thus, increasing electrode thickness increases the total capacity but also affects the amount of lithium plating that occurs. All of this can be noticed in Figure 46 below. --

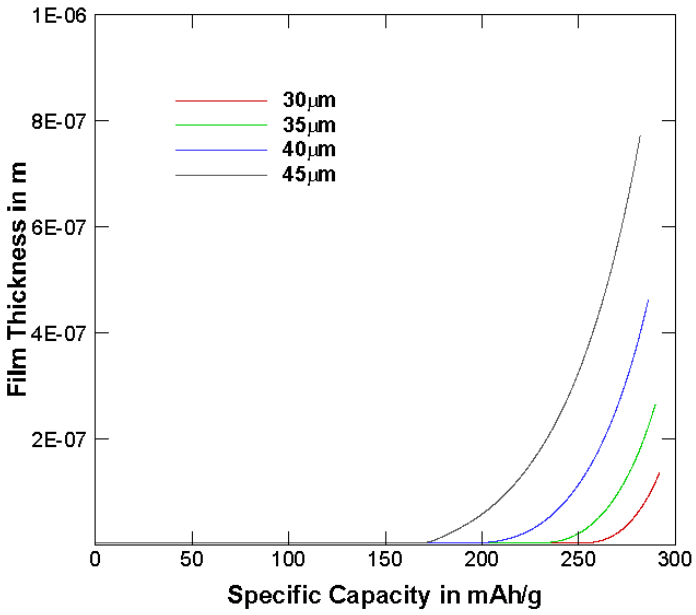

Figure 46: Lithium plating film thickness vs specific capacity at 255K

Conclusion

This chapter looked at the effect various parameters such as C-rate, temperature and electrode thickness has on the lithium plating that occurs. It was clear from the above studies that C-rate and temperature are equally influential in providing condition conducive to lithium plating. Electrode thickness and active material change affects the amount of lithium and current density thereby affecting the extent to which the electrode experiences lithium plating. Lithium plating is irreversible in nature and causes a depletion of the specific capacity of the electrode. Once plating begins, the rate of increase of the film thickness is exponential and can lead to a very quick reduction in the capacity of the battery system. Thus, extreme care must be taken to avoid the initiation of lithium plating in high C-rate or low temperature applications.

CHAPTER VII

CONCLUSIONS AND FUTURE SCOPE

Thermodynamically consistent models have been successfully created for positive electrodes with no phase change and for negative electrodes with multiple phase change regions. The phase change has been captured. Lithium plating has also been incorporated with a thermodynamically consistent model.

The thermodynamically consistent solid-state diffusivity was obtained by firstly fitting the open circuit potential vs state of charge to obtain the thermodynamically consistent fitting parameters. These parameters were then used to obtain a thermodynamically consistent solid-state diffusivity function that changed with change in the state of charge of the electrode. The solid-state diffusivity is highest at high states of lithiation. This is because the diffusion not only occurs on a particle-by-particle basis but also through the bulk movement of the intercalated species in the electrode. This is visualized as a wave of intercalation that sweeps across the electrode during intercalation.

Positive electrodes have no phase change observed with the exception of $LiFePO_4$. This can be corroborated through the fact that the open circuit potential for the positive electrodes under consideration (Nickel-Cobalt-Aluminum oxide) had no plateau. The thermodynamically consistent model was compared to the constant diffusivity model. At low C-rates, there isn't much of a difference between the two approaches due to the low intercalation overpotential. As C-rate is increased, the deviation of the constant diffusivity model from the thermodynamically consistent model can be seen, especially at high states

of lithiation. This is because of the assumption that diffusivity improves in thermodynamically consistent model. Under discharge, improved capacity utilization can be seen. This would imply a reduced utilization under charge.

For negative electrodes, there occurs phase change. The phases that are discussed in this study are LiC_6, LiC_{12} and LiC_{32}. Thermodynamically consistent approach was applied independently to each phase of the model by fitting the phase specific open circuit potential with the Nernst equilibrium potential function with excess chemical potential associated with intercalation. The effect of C-rate, electrode thickness, active material concentration and particle size were observed and the trends explained. The effect of these parameters on phase change were however interesting footnotes. To understand how phase change is affected by these parameters will help in modelling an electrode microstructure that is appropriate to the type of phase existing in the material.

The effect of the thermodynamically consistent model on plating was also discussed. The thermodynamically consistent modelling suggests reduced specific capacity with charge. It also suggests reduced capacity and phase change at higher C-rates. An increase in C-rate increases the overpotential at points where the solid-state potential is lesser than the electrolyte potential, plating is observed to occur on the surface of the electrode. Increasing C-rate increases the likelihood of plating occurring and decreasing temperature has the same effect. This was found to be true even in a thermodynamically consistent model but the extent to which plating occurs can be more accurately depicting using the phase change model.

The future scope of this project would be to incorporate phase change in the charging model and understand how phase change changes when lithium plating occurs. Another avenue to probe is the effect of lithium plating with particle size and electrode thickness.

NOMENCLATURE

a	Specific Interfacial area, 1/m
c	Concentration, mol/m3
D	Diffusivity coefficient, m^2/s
E	Equilibrium potential, V
F	Faraday's constant, C/mol
H(x)	Heaviside function
j	Volumetric electrochemical reaction flux, A/m^3
J	Surface reaction flux density, A/m^2
k	Reaction rate constant, $mol^{0.7}m^{-1.1}s^{-1}$
M	Molecular weight of Lithium metal, g/mol
r	Radial Co-ordinate, m
R	Universal Gas Constant, J/mol-K
R_p	Radius of isotropic electrode sphere
t	Time, s
t^+	Transference number of Lithium ion
T	Temperature, K
T_0	Reference Temperature, 298 K
x	State of Charge of species

Greek Symbols

γ	Activity coefficient, m^3
δ	Thickness of Lithium plating, m
Δ	Difference between final and initial states
ε	Volume fraction
$\varepsilon_{s,j}$	Phase specific volume fraction
κ_{junc}	Liquid junction electrolytic conductivity, S/m
κ_{eff}	Effective electrolytic conductivity, S/m
μ	Chemical potential, J
ν	Liquid thermodynamic co-efficient
ρ	Density of Lithium metal, kg/m^3
ϕ	Chemical potential, V
σ_{eff}	Effective electrode electronic conductivity, S/m
Ω	Fitting parameter

Subscripts

*	Supersaturation for phase nucleation
0	Reference state related to dilute limits
1	Intercalating species
2	Lithium plating terms
e	Electrolytic phase
eff	Effective

film	Lithium metal film
I	Intercalating species
j	Phase j
jk	Phase j to phase k transition
s	Solid phase
S	Vacant Site or host species

REFERENCES

1. *Estimated U.S Energy use in 2014*. 2015, Department of Energy.

2. Winter, M. and R.J. Brodd, *What are batteries, fuel cells, and supercapacitors?* 2004, ACS Publications.

3. Verma, P., P. Maire, and P. Novák, *A review of the features and analyses of the solid electrolyte interphase in Li-ion batteries.* Electrochimica Acta, 2010. **55**(22): p. 6332-6341.

4. Cairns, E.J. and P. Albertus, *Batteries for electric and hybrid-electric vehicles.* Annual Review of Chemical and Biomolecular Engineering, 2010. **1**: p. 299-320.

5. Dahn, J.R., et al., *Mechanisms for lithium insertion in carbonaceous materials.* Science, 1995. **270**(5236): p. 590.

6. Peled, E., *The electrochemical behavior of alkali and alkaline earth metals in nonaqueous battery systems—the solid electrolyte interphase model.* Journal of The Electrochemical Society, 1979. **126**(12): p. 2047-2051.

7. Rahn, C.D. and C.-Y. Wang, *Battery systems engineering*. 2013: John Wiley & Sons.

8. Ramadass, P., et al., *Capacity fade of Sony 18650 cells cycled at elevated temperatures: Part I. Cycling performance.* Journal of power sources, 2002. **112**(2): p. 606-613.

9. Ramadass, P., et al., *Mathematical modeling of the capacity fade of Li-ion cells.* Journal of Power Sources, 2003. **123**(2): p. 230-240.

10. Santhanagopalan, S., et al., *Review of models for predicting the cycling performance of lithium ion batteries.* Journal of Power Sources, 2006. **156**(2): p. 620-628.

11. Zhang, Q. and R.E. White, *Capacity fade analysis of a lithium ion cell.* Journal of Power Sources, 2008. **179**(2): p. 793-798.

12. van Schalkwijk, W. and B. Scrosati, *Advances in lithium-ion batteries*. 2007: Springer Science & Business Media.

13. Tarascon, J.-M. and M. Armand, *Issues and challenges facing rechargeable lithium batteries.* Nature, 2001. **414**(6861): p. 359-367.

14. Etacheri, V., et al., *Challenges in the development of advanced Li-ion batteries: a review.* Energy & Environmental Science, 2011. **4**(9): p. 3243-3262.

15. Besenhard, J., J. Yang, and M. Winter, *Will advanced lithium-alloy anodes have a chance in lithium-ion batteries?* Journal of Power Sources, 1997. **68**(1): p. 87-90.

16. Yoshio, M., R.J. Brodd, and A. Kozawa, *Lithium-ion batteries*. Vol. 1. 2009: Springer.

17. Yamada, A., S.-C. Chung, and K. Hinokuma, *Optimized LiFePO4 for lithium battery cathodes.* Journal of the electrochemical society, 2001. **148**(3): p. A224-A229.

18. Huang, H., S.-C. Yin, and L.s. Nazar, *Approaching theoretical capacity of LiFePO4 at room temperature at high rates.* Electrochemical and Solid-State Letters, 2001. **4**(10): p. A170-A172.

19. Bloom, I., et al., *Differential voltage analyses of high-power lithium-ion cells. 4. Cells containing NMC.* Journal of Power Sources, 2010. **195**(3): p. 877-882.

20. Kim, T.H., et al., *The current move of lithium ion batteries towards the next phase.* Advanced Energy Materials, 2012. **2**(7): p. 860-872.

21. Fang, W., O.J. Kwon, and C.Y. Wang, *Electrochemical–thermal modeling of automotive Li-ion batteries and experimental validation using a three-electrode cell.* International journal of energy research, 2010. **34**(2): p. 107-115.

22. Delmas, C., et al., *Lithium deintercalation in LiFePO4 nanoparticles via a domino-cascade model.* Nature materials, 2008. **7**(8): p. 665-671.

23. Xia, Y. and M. Yoshio, *An Investigation of Lithium Ion Insertion into Spinel Structure Li-Mn-O Compounds.* Journal of The Electrochemical Society, 1996. **143**(3): p. 825-833.

24. Van der Ven, A. and G. Ceder, *Lithium diffusion mechanisms in layered intercalation compounds.* Journal of power sources, 2001. **97**: p. 529-531.

25. Doyle, M., et al., *Comparison of modeling predictions with experimental data from plastic lithium ion cells.* Journal of the Electrochemical Society, 1996. **143**(6): p. 1890-1903.

26. Nagarajan, G.S., J. Van Zee, and R. Spotnitz, *A Mathematical Model for Intercalation Electrode Behavior I. Effect of Particle-Size Distribution on Discharge Capacity.* Journal of the Electrochemical Society, 1998. **145**(3): p. 771-779.

27. Doyle, M., T.F. Fuller, and J. Newman, *Modeling of galvanostatic charge and discharge of the lithium/polymer/insertion cell.* Journal of the Electrochemical Society, 1993. **140**(6): p. 1526-1533.

28. Arora, P., et al., *Comparison between computer simulations and experimental data for high-rate discharges of plastic lithium-ion batteries.* Journal of power Sources, 2000. **88**(2): p. 219-231.

29. Verbrugge, M.W. and B.J. Koch, *Electrochemical analysis of lithiated graphite anodes.* Journal of The Electrochemical Society, 2003. **150**(3): p. A374-A384.

30. Srinivasan, V. and J. Newman, *Discharge model for the lithium iron-phosphate electrode.* Journal of the Electrochemical Society, 2004. **151**(10): p. A1517-A1529.

31. Gomadam, P.M., et al., *Mathematical modeling of lithium-ion and nickel battery systems.* Journal of Power Sources, 2002. **110**(2): p. 267-284.

32. Zhang, X., A.M. Sastry, and W. Shyy, *Intercalation-induced stress and heat generation within single lithium-ion battery cathode particles.* Journal of The Electrochemical Society, 2008. **155**(7): p. A542-A552.

33. Schmidt, A.P., et al., *Experiment-driven electrochemical modeling and systematic parameterization for a lithium-ion battery cell.* Journal of Power Sources, 2010. **195**(15): p. 5071-5080.

34. Levi, M. and D. Aurbach, *Diffusion coefficients of lithium ions during intercalation into graphite derived from the simultaneous measurements and modeling of electrochemical impedance and potentiostatic intermittent titration characteristics of thin graphite electrodes.* The Journal of Physical Chemistry B, 1997. **101**(23): p. 4641-4647.

35. Jang, Y.-I., B.J. Neudecker, and N.J. Dudney, *Lithium Diffusion in Li x CoO2 (0.45< x< 0.7) Intercalation Cathodes.* Electrochemical and Solid-State Letters, 2001. **4**(6): p. A74-A77.

36. Prosini, P.P., et al., *Determination of the chemical diffusion coefficient of lithium in LiFePO 4.* Solid State Ionics, 2002. **148**(1): p. 45-51.

37. Yu, P., et al., *Determination of the lithium ion diffusion coefficient in graphite.* Journal of The Electrochemical Society, 1999. **146**(1): p. 8-14.

38. Bernardi, D.M., R. Chandrasekaran, and J.Y. Go, *Solid-state transport of lithium in lithium-ion-battery positive electrodes.* Journal of The Electrochemical Society, 2013. **160**(9): p. A1430-A1441.

39. Ji, Y., Y. Zhang, and C.-Y. Wang, *Li-ion cell operation at low temperatures.* Journal of The Electrochemical Society, 2013. **160**(4): p. A636-A649.

40. Fan, G., et al., *Modeling of Li-Ion cells for fast simulation of high C-Rate and low temperature operations.* Journal of The Electrochemical Society, 2016. **163**(5): p. A666-A676.

41. Senyshyn, A., et al., *Lithium intercalation into graphitic carbons revisited: Experimental evidence for twisted bilayer behavior.* Journal of The Electrochemical Society, 2013. **160**(5): p. A3198-A3205.

42. Yuan, L.-X., et al., *Development and challenges of LiFePO 4 cathode material for lithium-ion batteries.* Energy & Environmental Science, 2011. **4**(2): p. 269-284.

43. Baker, D.R. and M.W. Verbrugge, *Intercalate diffusion in multiphase electrode materials and application to lithiated graphite.* Journal of The Electrochemical Society, 2012. **159**(8): p. A1341-A1350.

44. Zhang, W.-J., *Lithium insertion/extraction mechanism in alloy anodes for lithium-ion batteries.* Journal of Power Sources, 2011. **196**(3): p. 877-885.

45. Huggins, R.A., *Materials science principles related to alloys of potential use in rechargeable lithium cells.* Journal of Power Sources, 1989. **26**(1-2): p. 109-120.

46. Gallagher, K.G., et al., *A volume averaged approach to the numerical modeling of phase-transition intercalation electrodes presented for LixC6.* Journal of The Electrochemical Society, 2012. **159**(12): p. A2029-A2037.

47. Bernardi, D.M. and J.-Y. Go, *Analysis of pulse and relaxation behavior in lithium-ion batteries.* Journal of Power Sources, 2011. **196**(1): p. 412-427.

48. Ohzuku, T., Y. Iwakoshi, and K. Sawai, *Formation of Lithium-Graphite Intercalation Compounds in Nonaqueous Electrolytes and Their Application as a Negative Electrode for a Lithium Ion (Shuttlecock) Cell.* Journal of The Electrochemical Society, 1993. **140**(9): p. 2490-2498.

49. Brunetti, G., et al., *Confirmation of the domino-cascade model by LiFePO4/FePO4 precession electron diffraction.* Chemistry of Materials, 2011. **23**(20): p. 4515-4524.

50. Sugar, J.D., et al., *High-resolution chemical analysis on cycled LiFePO 4 battery electrodes using energy-filtered transmission electron microscopy.* Journal of Power Sources, 2014. **246**: p. 512-521.

51. Chueh, W.C., et al., *Intercalation pathway in many-particle LiFePO4 electrode revealed by nanoscale state-of-charge mapping.* Nano letters, 2013. **13**(3): p. 866-872.

52. Li, Y., et al., *Current-induced transition from particle-by-particle to concurrent intercalation in phase-separating battery electrodes.* Nature materials, 2014. **13**(12): p. 1149-1156.

53. Ferguson, T.R. and M.Z. Bazant, *Phase transformation dynamics in porous battery electrodes.* Electrochimica Acta, 2014. **146**: p. 89-97.

54. Ferguson, T.R. and M.Z. Bazant, *Nonequilibrium thermodynamics of porous electrodes.* Journal of The Electrochemical Society, 2012. **159**(12): p. A1967-A1985.

55. Dargaville, S. and T.W. Farrell, *Predicting active material utilization in LiFePO4 electrodes using a multiscale mathematical model.* Journal of the Electrochemical Society, 2010. **157**(7): p. A830-A840.

56. Bazant, M.Z., *Theory of chemical kinetics and charge transfer based on nonequilibrium thermodynamics.* Accounts of chemical research, 2013. **46**(5): p. 1144-1160.

57. Latz, A. and J. Zausch, *Thermodynamic consistent transport theory of Li-ion batteries.* Journal of Power Sources, 2011. **196**(6): p. 3296-3302.

58. Colclasure, A.M. and R.J. Kee, *Thermodynamically consistent modeling of elementary electrochemistry in lithium-ion batteries.* Electrochimica Acta, 2010. **55**(28): p. 8960-8973.

59. Bower, A.F., P.R. Guduru, and V.A. Sethuraman, *A finite strain model of stress, diffusion, plastic flow, and electrochemical reactions in a lithium-ion half-cell.* Journal of the Mechanics and Physics of Solids, 2011. **59**(4): p. 804-828.

60. Smart, M. and B. Ratnakumar, *Effects of electrolyte composition on lithium plating in lithium-ion cells.* Journal of The Electrochemical Society, 2011. **158**(4): p. A379-A389.

61. Gireaud, L., et al., *Lithium metal stripping/plating mechanisms studies: a metallurgical approach.* Electrochemistry communications, 2006. **8**(10): p. 1639-1649.

62. Bugga, R.V. and M.C. Smart, *Lithium plating behavior in lithium-ion cells.* ECS Transactions, 2010. **25**(36): p. 241-252.

63. Zinth, V., et al., *Lithium plating in lithium-ion batteries at sub-ambient temperatures investigated by in situ neutron diffraction.* Journal of Power Sources, 2014. **271**: p. 152-159.

64. Petzl, M. and M.A. Danzer, *Nondestructive detection, characterization, and quantification of lithium plating in commercial lithium-ion batteries.* Journal of Power Sources, 2014. **254**: p. 80-87.

65. Unocic, R.R., et al., *Direct visualization of solid electrolyte interphase formation in lithium-ion batteries with in situ electrochemical transmission electron microscopy.* Microscopy and Microanalysis, 2014. **20**(04): p. 1029-1037.

66. Arai, J., et al., *In situ solid state 7Li NMR observations of lithium metal deposition during overcharge in lithium ion batteries.* Journal of The Electrochemical Society, 2015. **162**(6): p. A952-A958.

67. Brissot, C., et al., *In situ study of dendritic growth inlithium/PEO-salt/lithium cells.* Electrochimica acta, 1998. **43**(10): p. 1569-1574.

68. Zeng, Z., et al., *Visualization of electrode–electrolyte interfaces in LiPF6/EC/DEC electrolyte for lithium ion batteries via in situ TEM.* Nano letters, 2014. **14**(4): p. 1745-1750.

69. Park, G., et al., *The study of electrochemical properties and lithium deposition of graphite at low temperature.* Journal of Power Sources, 2012. **199**: p. 293-299.

70. Ge, H., et al., *Investigating Lithium Plating in Lithium-Ion Batteries at Low Temperatures Using Electrochemical Model with NMR Assisted Parameterization.* Journal of The Electrochemical Society, 2017. **164**(6): p. A1050-A1060.

71. Purushothaman, B. and U. Landau, *Rapid charging of lithium-ion batteries using pulsed currents a theoretical analysis.* Journal of The Electrochemical Society, 2006. **153**(3): p. A533-A542.

72. Arora, P., M. Doyle, and R.E. White, *Mathematical Modeling of the Lithium Deposition Overcharge Reaction in Lithium-Ion Batteries Using Carbon-Based Negative Electrodes.* Journal of the Electrochemical Society, 1999. **146**(10): p. 3543-3553.

73. Perkins, R.D., et al., *Controls oriented reduced order modeling of lithium deposition on overcharge.* Journal of Power Sources, 2012. **209**: p. 318-325.

74. Legrand, N., et al., *Physical characterization of the charging process of a Li-ion battery and prediction of Li plating by electrochemical modelling.* Journal of Power Sources, 2014. **245**: p. 208-216.

75. Tippmann, S., et al., *Low-temperature charging of lithium-ion cells part I: Electrochemical modeling and experimental investigation of degradation behavior.* Journal of Power Sources, 2014. **252**: p. 305-316.

76. Mukherjee, P.P., S. Pannala, and J.A. Turner, *Modeling and simulation of battery systems.* Handbook of Battery Materials, Second Edition, 2011: p. 841-875.

77. Verbrugge, M.W. and B.J. Koch, *Modeling lithium intercalation of single-fiber carbon microelectrodes.* Journal of The Electrochemical Society, 1996. **143**(2): p. 600-608.

78. Zhang, J., et al., *Comparison and validation of methods for estimating heat generation rate of large-format lithium-ion batteries.* Journal of Thermal Analysis and Calorimetry, 2014. **117**(1): p. 447-461.

79. Sato, N., *Thermal behavior analysis of lithium-ion batteries for electric and hybrid vehicles.* Journal of power sources, 2001. **99**(1): p. 70-77.

80. Valøen, L.O. and J.N. Reimers, *Transport properties of LiPF6-based Li-ion battery electrolytes.* Journal of The Electrochemical Society, 2005. **152**(5): p. A882-A891.

81. Newman, J. and K.E. Thomas-Alyea, *Electrochemical systems*. 2012: John Wiley & Sons.

82. Dees, D., et al., *Electrochemical modeling of lithium-ion positive electrodes during hybrid pulse power characterization tests.* Journal of the Electrochemical Society, 2008. **155**(8): p. A603-A613.

83. Dahn, J., *Phase diagram of Li x C 6.* Physical Review B, 1991. **44**(17): p. 9170.

84. Chen, Y.-H., et al., *Selection of conductive additives in li-ion battery cathodes a numerical study.* Journal of the Electrochemical Society, 2007. **154**(10): p. A978-A986.

85. Gupta, A.K., *Regression and Model Fitting*, in *Numerical Methods using MATLAB*. 2014, Springer. p. 107-118.

86. Zheng, H., et al., *A comprehensive understanding of electrode thickness effects on the electrochemical performances of Li-ion battery cathodes.* Electrochimica Acta, 2012. **71**: p. 258-265.

87. Singh, M., J. Kaiser, and H. Hahn, *Thick electrodes for high energy lithium ion batteries.* Journal of The Electrochemical Society, 2015. **162**(7): p. A1196-A1201.

88. Xiang, X., X. Li, and W. Li, *Preparation and characterization of size-uniform Li [Li 0.131 Ni 0.304 Mn 0.565] O 2 particles as cathode materials for high energy lithium ion battery.* Journal of Power Sources, 2013. **230**: p. 89-95.

89. Mistry, A., et al., *Analysis of Long-Range Interaction in Lithium-Ion Battery Electrodes.* Journal of Electrochemical Energy Conversion and Storage, 2016. **13**(3): p. 031006.

90. Liu, G., et al., *Effects of various conductive additive and polymeric binder contents on the performance of a lithium-ion composite cathode.* Journal of The Electrochemical Society, 2008. **155**(12): p. A887-A892.

91. Fong, R., U. Von Sacken, and J.R. Dahn, *Studies of lithium intercalation into carbons using nonaqueous electrochemical cells.* Journal of The Electrochemical Society, 1990. **137**(7): p. 2009-2013.

92. Billaud, D., et al., *New results concerning the lithium-pyrographite system.* Synthetic Metals, 1981. **3**(1-2): p. 21-26.

93. Fischer, J. and H. Kim, *Staging transitions at constant concentration in intercalated graphite.* Synthetic Metals, 1985. **12**(1-2): p. 137-142.

94. Dillon, S.J. and K. Sun, *Microstructural design considerations for Li-ion battery systems.* Current Opinion in Solid State and Materials Science, 2012. **16**(4): p. 153-162.

95. Arthur, T.S., et al., *Three-dimensional electrodes and battery architectures.* Mrs Bulletin, 2011. **36**(07): p. 523-531.